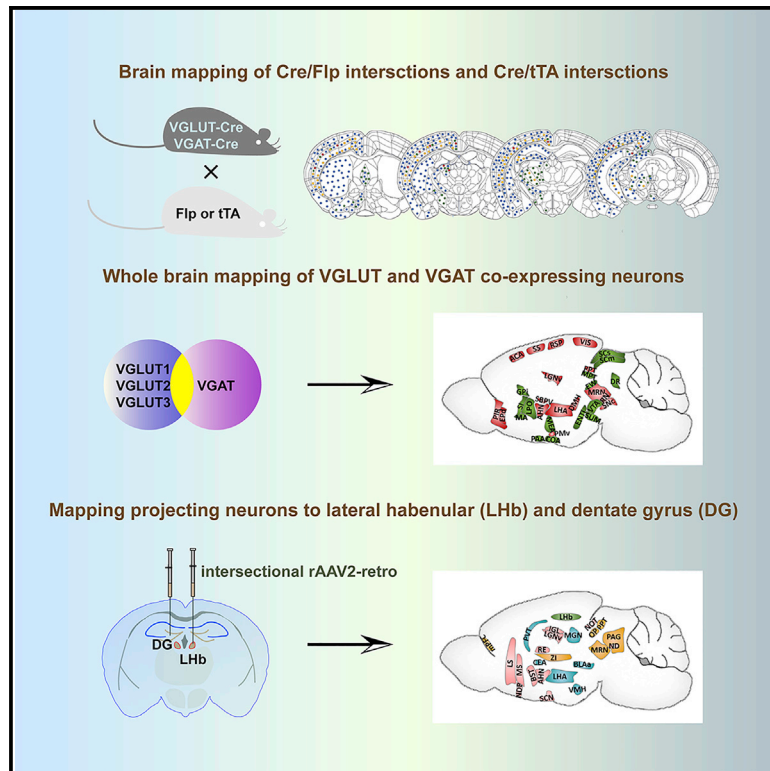# Intersectional mapping of multi-transmitter neurons and other cell types in the brain

Graphical abstract

Authors

Jian Xu, Andrew Jo, Raina P. DeVries, ..., Talia N. Lerner, Hongkui Zeng, Yongling Zhu

Correspondence

yongling-zhu@northwestern.edu

In brief

Xu et al. characterize Flp and tTA mouse driver lines, map VGLUT/VGAT co-expressing neurons in the brain, and trace LHb-projecting neurons along with the type of transmission. This study provides a resource for the future application of intersectional strategies and expands our understanding of glutamate/GABA co-releasing neurons in the brain.

Highlights

- Brain-wide characterization of 13 Flp and tTA mouse driver lines

- 30 brain regions contain neurons co-expressing VGLUT and VGAT

- 14 brain regions innervate the LHb with glutamate/GABA co-transmission

- LHb receives glutamatergic and/or GABAergic innervations from ~40 brain regions

CellPress

Resource

Intersectional mapping of multi-transmitter neurons and other cell types in the brain

Jian Xu,[1,2,7] Andrew Jo,[1,7] Raina P. DeVries,[4,7] Sercan Deniz,[1] Suraj Cherian,[1] Idris Sunmola,[1] Xingqi Song,[5] John J. Marshall,[2] Katherine A. Gruner,[3] Tanya L. Daigle,[6] Anis Contractor,[2] Talia N. Lerner,[2] Hongkui Zeng,[6] and Yongling Zhu[1,2,8,*]

[1]Departments of Ophthalmology and Neuroscience, Feinberg School of Medicine, Northwestern University, Chicago, IL 60611, USA
[2]Department of Neuroscience, Feinberg School of Medicine, Northwestern University, Chicago, IL 60611, USA
[3]Mouse Histology and Phenotyping Laboratory, Northwestern University, Chicago, IL 60611, USA
[4]Department of Organismal Biology and Anatomy, The University of Chicago, Chicago, IL 60637, USA
[5]School of Medicine, Shanghai Jiao Tong University, Shanghai 200240, China
[6]Allen Institute for Brain Science, Seattle, WA 98109, USA
[7]These authors contributed equally
[8]Lead contact
*Correspondence: yongling-zhu@northwestern.edu
https://doi.org/10.1016/j.celrep.2022.111036

SUMMARY

Recent developments in intersectional strategies have greatly advanced our ability to precisely target brain cell types based on unique co-expression patterns. To accelerate the application of intersectional genetics, we perform a brain-wide characterization of 13 Flp and tTA mouse driver lines and selected seven for further analysis based on expression of vesicular neurotransmitter transporters. Using selective Cre driver lines, we created more than 10 Cre/tTA combinational lines for cell type targeting and circuit analysis. We then used VGLUT-Cre/VGAT-Flp combinational lines to identify and map 30 brain regions containing neurons that co-express vesicular glutamate and gamma-aminobutyric acid (GABA) transporters, followed by tracing their projections with intersectional viral vectors. Focusing on the lateral habenula (LHb) as a target, we identified glutamatergic, GABAergic, or co-glutamatergic/GABAergic innervations from ∼40 brain regions. These data provide an important resource for the future application of intersectional strategies and expand our understanding of the neuronal subtypes in the brain.

INTRODUCTION

The mammalian brain contains millions or billions of neurons (70 million/mouse, 8.6 billion/human), which must be wired into specific circuits to execute computations. Given these large numbers, unsurprisingly, the precise number of cell types in many brain regions remains unknown. While recent advances in single-cell analysis (Cowan et al., 2020; Hodge et al., 2019; Kim et al., 2020; Peng et al., 2019; Tasic et al., 2016, 2018; Yao et al., 2021; Yuste et al., 2020) provide gene expression patterns that can be used for neuron type enumeration and selective targeting, using single genes to target defined populations of neurons can be problematic, insofar as Cre drivers controlled by specific gene promoters can be expressed in multiple cell types in a defined structure (Kim et al., 2017; Marterssteck et al., 2017; Taniguchi et al., 2011; Zhu et al., 2014). Thus, in many cases, the expression patterns in Cre driver lines must be further refined in order to segregate cell types. Intersectional strategies that use two or more orthogonal binary systems such as Cre/loxP, Flp/FRT (Broach et al., 1982; Dymecki et al., 2010), and tTA/TRE (Gossen and Bujard, 1992) can increase targeting specificity and lead to the identification of neuron types with novel functions (Daigle et al., 2018; He et al., 2016; Jo et al.,

2018; Madisen et al., 2015; Poulin et al., 2018; Ren et al., 2019). The successful exploitation of intersectional genetics relies on three recent and ongoing innovations: an increasing number of Flp and tTA driver lines, reporter/effector mouse lines for Cre/Flp and Cre/tTA intersections (Daigle et al., 2018; He et al., 2016; Madisen et al., 2015), and intersectional reporter viral vectors (Fenno et al., 2014, 2020). Since the expression patterns of relatively few Flp and tTA driver lines have been characterized and viral and genetic reporters for intersections have only recently been described, examples of studying neurons based on intersectional expression patterns are still limited.

An important step towards the effective use of intersectional strategies is the characterization of driver lines. This characterization not only can validate Flp and tTA expression patterns but can also serve as an important reference to help design appropriate intersections and discover novel cell types. Here, we present a brain-wide characterization of 13 Flp and tTA driver lines. We then selected seven of them and segregated the targeted neurons based on their expression of either of the vesicular glutamate transporter genes VGLUT1, VGLUT2, VGLUT3 or the vesicular gamma-aminobutyric acid (GABA) transporter VGAT. Based on the characterization, we created Cre/tTA intersections to boost efficiencies of reporters and effectors for

functional studies. These mouse lines expand existing intersectional tools and provide useful resources for studying specific cell types and circuits.

Many neurons can produce, store, and release multiple neurotransmitters. Intersectional strategies are particularly powerful in the mapping of brain-wide distributions of these multi-transmitter neurons based on the expression of genes needed to establish neurotransmitter identity. In this study, we performed a brain-wide mapping of neurons that are potentially capable of co-releasing glutamate and GABA. By creating intersections between VGLUT (VGLUT1, VGLUT2, or VGLUT3) and VGAT, we identified ∼30 brain regions containing VGLUT2/VGAT or VGLUT3/VGAT co-expressing neurons in the adult. Viral tracing further revealed ∼70% of the regions containing VGLUT2/VGAT co-expressing neurons innervated the lateral habenula (LHb) with glutamate/GABA co-transmission. These results reveal an unanticipated abundance of glutamate/GABA co-transmission in the brain and add to our understanding of the afferent circuitry to the LHb.

RESULTS

Expression patterns of Flp drivers and tTA drivers

We started by screening seven Flp drivers (SST-FlpO, VIP-FlpO, Pvalb-FlpE, Dlx5/6-FlpO, Rasgrf2-FlpO, Rorb-FlpO, and Nkx2-FlpO) and six tTA drivers (Camk2a-tTA, Scg2-tTA, Rorb-tTA, NEFH-tTA, DAT-tTA, and Rosa-LNL-tTA). We crossed each line with a ubiquitous CMV-Cre driver and a reporter line (Ai65 for the Cre/Flp intersection, Ai62 for the Cre/tTA intersection).

All of the Flp drivers labeled isocortical neurons. Rorb-FlpO and Rasgrf2-FlpO showed restricted labeling, while the other five lines showed widespread labeling in all layers. Except for Rorb-FlpO, every Flp driver labeled subcortical neurons. Pvalb, SST, and VIP are major genetic markers for GABAergic neurons in the cortex and could also be important markers for subcortical neurons, thus we focused our follow-up analysis (see below) on these three Flp driver lines.

The six tTA drivers can be separated into three groups: (1) Rorb-tTA-labeled neurons were restricted to L4 of the primary sensory cortex in line with expectation insofar as Rorb is an established genetic marker for this area (Hawrylycz et al., 2010; Zhuang et al., 2017). (2) DAT-tTA only labeled subcortical neurons and avoided cortical regions and the hippocampus. (3) Rosa-LNL-tTA, Camk2a-tTA, Scg2-tTA, and NEFH-tTA labeled both cortical and subcortical neurons. We selected Camk2a-tTA, Scg2-tTA, NEFH-tTA, and Rorb-tTA for further intersectional analysis.

The results of Rorb-FlpO, Rasgrf2-FlpO, Dlx5/6-FlpO, Nkx2-FlpO, DAT-tTA, and Rosa-LNL-tTA are shown in Figures S1 and S2.

Segregation of glutamatergic and GABAergic neurons in Flp driver lines and tTA driver lines

Based on the initial screen, three Flp lines (Pvalb, SST, and VIP) and four tTA lines (CaMk2a-tTA, Scg2-tTA, NEFH-tTA, and Rorb-tTA) were selected for further analysis. To further segregate Flp⁺ or tTA⁺ neurons, we crossed each Flp or tTA line with four neurotransmitter transporter Cre lines: VGLUT1-Cre, VGLUT2-Cre, VGLUT3-Cre, and VGAT-Cre. This strategy allowed us to separate Flp- or tTA-labeled neurons into four categories based on the expression of the four neurotransmitter transporters. Accordingly, we generated 28 intersectional Cre/Flp and Cre/tTA mouse lines that were each crossed with appropriate reporter lines for target cell identification (Figures 1A and 2A).

GABAergic and glutamatergic neurons in Flp driver lines

Isocortical regions. The results are summarized in Figures 1B–1D and Table S2. As expected, the vast majority of neurons in Pvalb-FlpE and SST-FlpO drivers, and all the neurons in the VIP-FlpO driver, were GABAergic, as revealed by their intersections with VGAT-Cre. Against expectation, small subsets of glutamatergic neurons were also revealed in several intersections. We examined the expression of Pvalb, SST, or VIP in the labeled cells with immunohistochemistry, and summarized the results in Table S2.

The VGLUT1/Pvalb intersection labeled clusters of L5 neurons in primary somatosensory cortex (SSp), as well as L5 and L2/3 neurons in the retrosplenial cortex (RSP) (Figure 1E). The labeling was excluded from the primary visual cortex (VISp) and was sparse in L5 of the anterolateral visual cortex (VISal) (Figures 1E and S3A). The morphology of the cells in SSp suggested they were pyramidal tract (PT) corticofugal neurons. This suggestion is further supported by the labeled axonal projections in the striatum, thalamus, subthalamic nucleus (STN), and superior colliculus (SC) (Figure S3A). Pvalb was likely expressed in these neurons only transiently during development as immunohistochemistry showed no or very weak Pvalb expression in the adult (Figure S4A). The VGLUT2/Pvalb intersection showed the same labeling pattern as the VGLUT1/Pvalb intersection, presumably due to a developmental switch from VGLUT2 to VGLUT1 in the cortex (Boulland et al., 2004; Fremeau et al., 2004).

VGLUT1/SST and VGLUT2/SST intersections both labeled a subset of neurons in the primary motor cortex (MOp). The somas of these neurons were in L6, but their dendrites spanned across L5 and L6 (Figure 1F). Their horizontal axons projected to L5 and L6 of the somatosensory cortex (SSp and SSs) and the corpus callosum. Based on the morphology and projection, they are likely to be cortico-cortical (CC) pyramidal cells, but some claustrum projecting pyramidal cells might also be labeled. A population of pyramidal neurons in the piriform cortex (PIR) was also labeled in the VGLUT1/SST and VGLUT2/SST intersections (Figure S5A). However, immunohistochemistry showed no SST expression in these MOp and PIR pyramidal cells in the adult, suggesting SST was probably transiently expressed in these cells during development.

VGLUT3/Pvalb and VGLUT3/SST intersections labeled L6 and L5 neurons in isocortex (Figures S3C and S5B). Immunohistochemistry revealed that a fraction of labeled neurons in the VGLUT3/Pvalb intersection expressed Pvalb (Figure S4D), but no SST expression was detected in the VGLUT3/SST intersection.

Allocortical and subcortical regions. We summarize the results in Table S2. GABAergic Pvalb or SST neurons were widely distributed in the subcortical regions, as revealed in the VGAT-Cre/Pvalb-FlpE and VGAT-Cre/SST-FlpO intersections (Figures 1B,
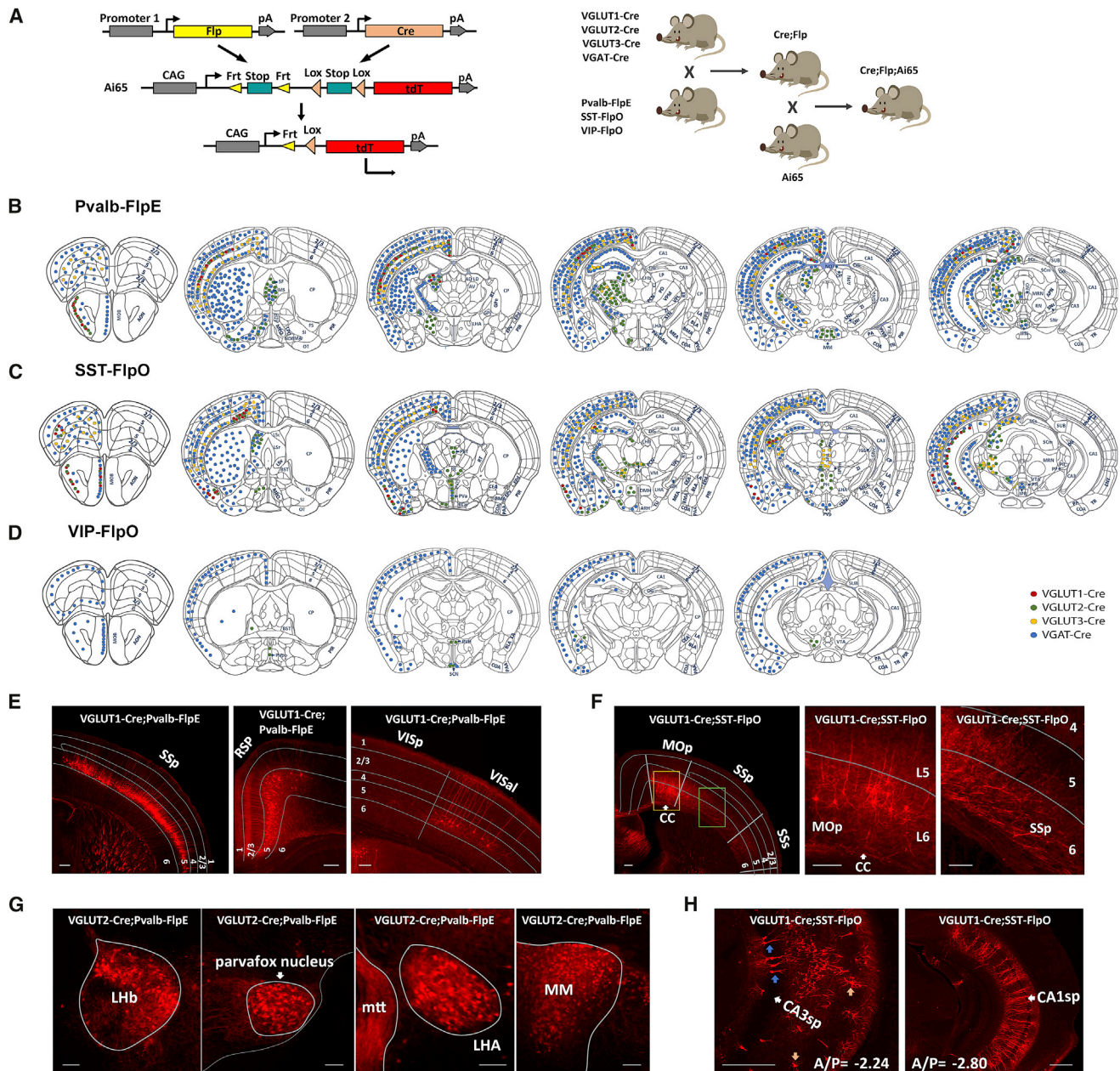
Figure 1. Analysis of Flp drivers with Cre/Flp intersectional strategy

(A) Left: Cre/Flp intersectional strategy. Right: triple transgenic breeding scheme for analyzing Flp drivers based on their expressions of different neurotransmitter transporters.

(B–D) Distributions of VGLUT1 (red), VGLUT2 (green), VGLUT3 (orange), or VGAT (blue) expressing neurons labeled in Pvalb-FlpE (B), SST-FlpO (C), and VIP-FlpO (D) drivers. See also Figures S3, S5, and Table S2 for more information.

(E) VGLUT1-Cre/Pvalb-FlpE intersection labeled a cluster of L5 neurons in the SSp and VISal, as well as L5 and L2/3 neurons in the RSP.

(F) VGLUT1-Cre/SST-FlpO labeled a subset of L6 and L5 neurons in the MOp. These neurons sent their horizontal axons to the corpus callosum (CC) and L6 of SS. The orange box and green box in the left panel are enlarged in the middle panel right panel respectively.

(G) Pvalb-expressing glutamatergic neurons in selected regions. See also Figures S3B, S4B, and S4C for more information.

(H) Left: Ai65 labeled pyramidal neurons (blue arrow) and interneurons (orange arrow) in the CA3 of the hippocampus. Right: Ai65 labeled pyramidal neurons in the CA1 of the hippocampus.

Scale bars: 200 μm (E and F), 100 μm (G), 500 μm (H).

1C, S3D, and S5C). The reticular nucleus (RT) showed the most intense labeling in both intersections. Immunochemistry revealed that most Pvalb neurons expressed Pvalb in the adult (Table S2). GABAergic VIP neurons were scarce. The most intense labeling was observed in the suprachiasmatic nucleus (SCN) and main olfactory bulb (MOB) (Figures 1D and S3F). The distributions of GABAergic SST or VIP neurons were in agreement with their mRNA expression patterns described in the *in situ* hybridization Allen Mouse Brain Atlas (ABA-ISH, http://www.brain-map.org) (Lein et al., 2007). These results suggest that subcortical GABAergic Pvalb, SST, and VIP neurons express these marker proteins in the adult.

As expected, a majority of the glutamatergic Pvalb neurons were observed in VGLUT2/Pvalb intersections (Figures 1B and S3B). With antibody staining, we detected Pvalb expression in nine nuclei: LHb, lateral hypothalamic (LHA) parvafox nucleus, another LHA nucleus next to the mtt tract, medial mammillary nucleus (MM), olivary pretectal nucleus (OP), nucleus of Darkschewitsch (ND), red nucleus (RN), rostral interpeduncular nucleus (IPR), and sensory related SC (Figures 1G, S4B, and S4C). Pvalb$^+$ plexuses were also visualized in the ventral posteromedial nucleus (VPM) and ventral posterolateral nucleus (VPL) of the thalamus, although in these areas the somatic expression of Pvalb was largely not detected (Figure S4B). We speculate that the lack of somatic staining is caused by transport of Pvalb from somas to axons and dendrites.

One surprising observation was that a subset of hippocampal neurons in the dorsal CA3 and ventral CA1 were labeled in the VGLUT1-Cre/SST-FlpO intersection (Figure 1H). While the labeled neurons in the CA1 were exclusively pyramidal cells, the cells in the CA3 included both pyramidal neurons and interneurons. However, immunochemistry showed the labeled pyramidal neurons and interneurons did not express SST in the adult.

Additional SST neurons expressing VGLUT2 or VGLUT3 were observed in the thalamus, hypothalamus, and midbrain (Figures S5A and S5B; Table S2). However, except for the neurons in the LHb (VGLUT2/SST), GPi (VGLUT2/SST), VTA (VGLUT2/SST), and hippocampal CA3-so (VGLUT3/SST), most of these neurons do not express SST in the adult (ABA-ISH and immunochemistry in this study).

Glutamatergic and GABAergic neurons in tTA driver lines

We summarize the labeling patterns in Table S3.

Isocortical regions. In contrast to the Flp drivers, the four tTA drivers only labeled glutamatergic neurons in the cortex. As expected, the VGLUT1-Cre/Rob-tTA intersection exclusively labeled L4 neurons of the primary sensory cortex (SS, VIS, AUD, and GU) (Figures 2E). The VGLUT1-Cre (or VGLUT2-Cre) intersections with CaMk2a-tTA and Scg2-tTA predominately labeled L4 and L6 neurons in the primary sensory cortex (Figures 2B, 2C, S6A, S6D, and S6E). NEFH-tTA labeled L4 and L6 neurons in the primary sensory cortex, along with L6 neurons in other isocortical regions (Figures 2D, S7A, and S7B). Glutamatergic neurons in the piriform cortex were labeled in all the tTA drivers (Figures S6A, S6D, S6E, S7A, and S7B) except for Rorb-tTA.

VGLUT3-Cre intersected with CaMk2a-tTA, Scg2-tTA, and NEFH-tTA predominately labeled L4 and L6 neurons of the SS,

L6 neurons of the AUD and VIS, as well as L2/3 and L6 neurons of the MO (Figures 2B–2D, S6B, S6F, and S7C). No labeling was observed in the VGLUT3-Cre/Rorb-tTA intersection.

Allocortical and subcortical regions. All three tTA lines labeled glutamatergic neurons in the hippocampus, although labeling patterns differed (Figures 2B–2D, S6A, S6D, S6E, S7A, and S7B). CaMk2a-tTA and NEFH-tTA strongly labeled CA1, CA3, and DG neurons (Figures S6A, S7A, and S7B), while Scg2-tTA strongly labeled CA1 neurons but weakly labeled CA3 and DG neurons (Figures S6D and S6E). They all labeled glutamatergic neurons in the basolateral amygdala (BLA) (Figures S6A, S6D, S7A, and S7B) and endopiriform nucleus (EP) (Figures S6A and S6D). In addition, Scg2-tTA labeled the intralaminar nuclei of the thalamus and SNc (Figures S6D and S6E), and NEFH-tTA labeled the midline group of the dorsal thalamus, SNc, and VTA (Figure S7B).

Most of the GABAergic neurons labeled in the 3 tTA drivers were concentrated in the striatum, pallidum, amygdala, olfactory bulb, and SCN (Figures S6C, S6G, and S7D). Scg2-tTA also targeted GABAergic neurons in retinorecipient regions: the lateral geniculate nucleus (LGN), medial pretectal area (MPT), nucleus of the optic tract (NOT), OP, and SCs (Figure S6G).

NEFH-tTA labeled VGLUT3-expressing neurons in five nuclei of the thalamus (Figures 2D and S7C) where VGLUT3 mRNA is expressed (ABA-ISH). CaMk2a-tTA, Scg2-tTA, or NEFH-tTA also labeled VGLUT3 neurons in the CLA and EP (Figures S6B, S6F, and S7C) where VGLUT3 mRNA is absent (ABA-ISH), suggesting VGLUT3 expression in these cells was discontinued in the adult.

Cre/tTA intersections for restricted labeling and for more robust functional studies. We developed ~20 Cre/tTA mouse lines and selected 10 of them for further analysis based on reporter expression patterns and levels. These lines were generated with six Cre drivers crossed with either CaMk2a-tTA or Scg2-tTA (Figure 2F). We found that these combinational lines can be used to selectively target neuron populations in different subregions of the cortex (Figure 2G), hippocampus (Figure 2H), and amygdala (Figure 2I). The results are summarized in Table S4.

Neurons co-expressing VGLUT and VGAT

Although intersectional strategies can be used in many ways, an immediate and significant application is to map neurons conducting neurotransmitter co-release (Granger et al., 2017; Tritsch et al., 2016; Yang et al., 2021). Recent studies have presented evidence for glutamate and GABA co-release (Hashimotodani et al., 2018; Pedersen et al., 2017; Root et al., 2014, 2018; Shabel et al., 2014; Sonoda et al., 2020; Yoo et al., 2016). Dual excitatory and inhibitory fast transmitter release allows neurons to send opposite signals to different target, or to provide simultaneous excitation and inhibition to the same target. To examine the prevalence of neurons with the capability of co-releasing glutamate and GABA, we intersected VGAT-FlpO with VGLUT1-Cre, VGLUT2-Cre, or VGLUT3-Cre. Using these intersectional VGLUT/VGAT lines, we examined the distribution of VGLUT/VGAT double-positive neurons, evaluated the co-expression of VGLUTs and VGAT in the adult, and mapped their projections.
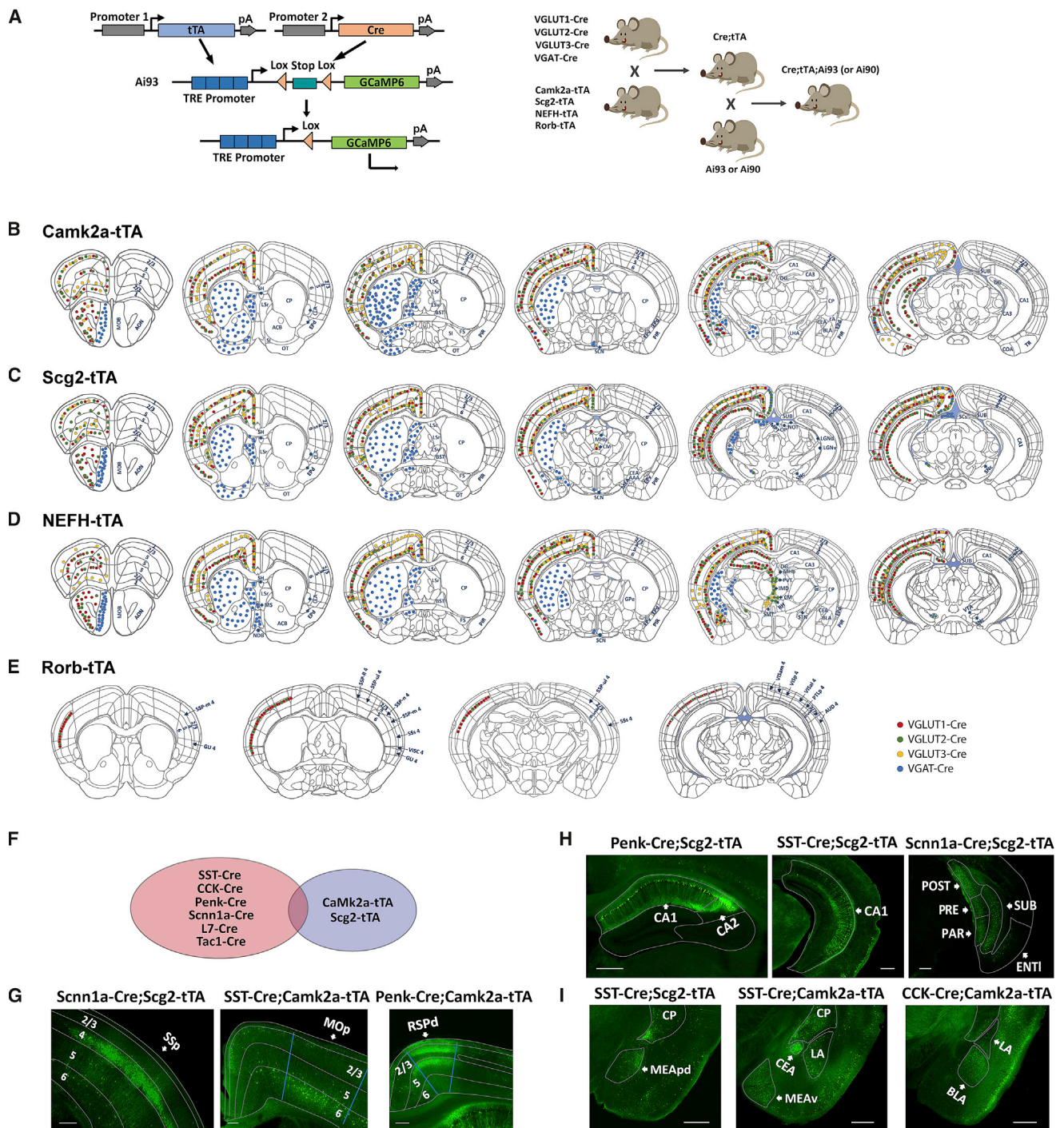
Figure 2. Characterization of tTA drivers with Cre/tTA intersectional strategy

(A) Left: Cre/tTA intersectional strategy. Right: triple transgenic breeding scheme for analyzing tTA drivers based on their expressions of neurotransmitter transporters.

(B–E) Distributions of VGLUT1 (red), VGLUT2 (green), VGLUT3 (orange), or VGAT (blue) expressing neurons labeled in Camk2a-tTA (B), Scg2-tTA (C), NEFH-tTA (D), and Rorb-tTA (E) drivers. See also Figures S6, S7, and Table S3 for more information.

(F–I) Cre/tTA intersections (F) allowed for selective targeting of neuron populations in the isocortex (G), hippocampus (H), and amygdalar (I). See also Table S4 for more information.

Scale bars: 200 μm (G), 500 μm (H and I).
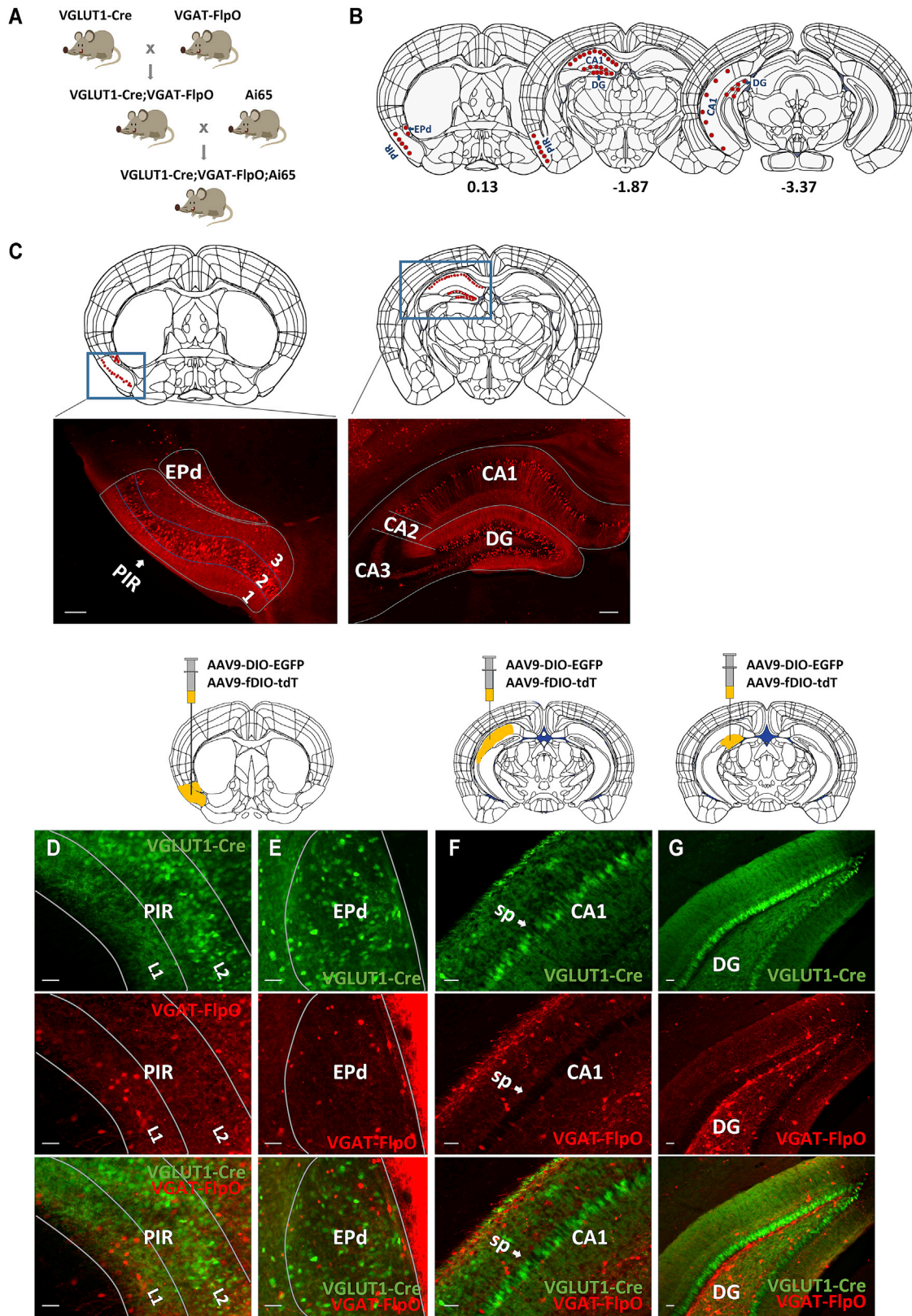
(legend on next page)

VGLUT1/VGAT intersections

In VGLUT1-Cre;VGAT-FlpO;Ai65 mice, the strongest labeling was observed in the pyramidal layer of the PIR and EPd (Figures 3B and 3C, left). Additional labeled neurons were observed in the pyramidal layer of the CA1 and in the granule cell layer of the DG in the hippocampus (Figures 3B and 3C, right).

Like many transgenic reporters, Ai65 can mark Cre/Flp intersections even if the recombinase only expresses transiently during development. Thus, we examined whether neurons reported by Ai65 continued to express Cre and Flp in the adult by injecting two sets of AAVs to VGlut1-Cre;VGAT-FlpO mice. In the first set, we injected INTRSECT AAV9-C_{on}/F_{on}-EYFP, which requires both Cre and Flp for expression of EYFP (Fenno et al., 2014). In the second set, we injected a mixture of AAV9-DIO-EGFP (Cre-dependent EGFP expression)/AAV9-fDIO-tdTomato (Flp-dependent tdTomato expression) and searched for neurons co-labeled with EGFP/tdTomato.

We found that AAV9-C_{on}/F_{on}-EYFP did not label any neurons in the PIR, EPd, CA1, and DG (data not shown). In the case of co-injection of AAV9-DIO-EGFP and AAV9-fDIO-tdTomato, all the four regions showed abundant EGFP-labeled VGLUT1-expressing neurons, but they showed no (Figures 3D, 3F, and 3G) or very few tdTomato-labeled cells (Figure 3E). Therefore, although VGLUT1 and VGAT were once expressed in the same neurons in these regions, VGAT was no longer expressed in the adult.

VGLUT2/VGAT intersections

In VGLUT2-Cre;VGAT-FlpO;Ai65 mice, tdTomato-labeled neurons were observed in ~37 brain regions (Figure 4B). Labeled neurons were densely packed in the globus pallidus internal segment (GPi), VTA, supramammillary nucleus (SUM), Edinger-Westphal nucleus (EW), substantia innominate (SI), and dorsomedial nucleus of the hypothalamus (DMH) (Figure 4C). Remarkably, in the LHb and DG (Figure 4D), we saw intense signals originating from axonal terminals, indicating these areas were heavily innervated by VGLUT2/VGAT co-expressing neurons, as previously reported (Hashimotodani et al., 2018; Pedersen et al., 2017; Root et al., 2014; Shabel et al., 2014).

To identify neurons that continued to co-express VGLUT2 and VGAT in the adult, we performed RNAScope dual in situ hybridization to detect both VGLUT2 and VGAT mRNAs simultaneously (Figure 4E). We found that among the 37 regions reported by Ai65, 19 regions contained neurons co-expressing VGLUT2 and VGAT, whereas the other 18 regions did not show any co-expression (Figure 4F). Eight of the co-expressing regions (GPi, IF, PN, PBP, RLi, SUM, DR, and CLi) have already been reported (Huang et al., 2019; Root et al., 2018; Soussi et al., 2010; Wallace et al., 2017), while the other 11 regions (SI, MA, LPO, MEA, COA, PAA, SCs, SCm, MPT, EW, and ENTl) (Figure 4E) have not. We

also confirmed VGLUT2/VGAT co-expression in these 19 regions by EYFP expression mediated by AAV9-C_{on}/F_{on}-EYFP injected into VGLUT2-Cre/VGAT-FlpO mice (data not shown). A summary of the regions that continued to co-express VGLUT2/VGAT versus those that no longer express is presented in Figure 4F.

Given the intense labeling of axonal terminals in the LHb and DG, we decided to map the neurons of origin in the whole brain. We injected two sets of retrograde AAVs in the LHb or DG of VGLU2-Cre;VGAT-FlpO mice (Figure 5A): (1) AAV2-retro-C_{on}/F_{on}-EYFP that labels VGLUT2/VGAT projecting neurons with a single color (EYFP); and (2) a mixture of AAV2-retro-DIO-EGFP/AAV2-retro-fDIO-tdTomato that labels VGLUT2 projecting neurons with EGFP, VGAT projecting neurons with tdTomato, and VGLUT2/VGAT projecting neurons with EGFP and tdTomato. In agreement with previous reports (Root et al., 2014; Shabel et al., 2014), retrograde tracing from the LHb with AAV2-retro-C_{on}/F_{on}-EYFP identified a large number of VGLUT2/VGAT neurons in the GPi and VTA (Figure 5B). Although AAV2-retro-C_{on}/F_{on}-EYFP worked effectively to map VGLUT2/VGAT neurons, we reasoned co-injection of AAV2-retro-DIO-EGFP/AAV2-retro-fDIO-tdTomato may be even better for this application because a single injection would label three populations of projecting neurons.

This was indeed the case. We made two discoveries with co-injection of AAV2-retro-DIO-EGFP/AAV2-retro-fDIO-tdTomato into the LHb. First, in addition to the GPi and VTA (IF, PN, PBP, RLi, CLi), eight more structures contained VGLUT2/VGAT neurons projecting to the LHb. These structures include EW (data not shown) and the seven structures shown in Figure 5C: SI and magnocellular nucleus (MA) of the ventral pallidum (PALv), sublayer a of posterodorsal medial amygdala nucleus (MEApd-a), cortical amygdala area (COA), lateral preoptic area (LPO), optic layer of sensory related SC (SCs-op), and MPT. Therefore, the LHb received glutamatergic/GABAergic co-innervation from broader regions of the brain than expected. Second, these 14 regions marked by retro-AAV not only provided glutamatergic/GABAergic co-innervation but also contained neurons providing sole glutamatergic innervation or sole GABAergic innervation to the LHb (Figure 5C). Among these regions, projections from the EW, MEA, and COA to the LHb have not been demonstrated before. We estimated the fractions of sole glutamatergic innervation, sole GABAergic innervation, and glutamatergic/GABAergic co-innervation from each projecting area and present the results in Figure 5D and Table S5. The results revealed four features of LHb projection from these areas. First, ~90% of projecting neurons from the GPi and IF innervated the LHb with glutamate/GABA co-transmission. This fraction was the highest among all regions that project of LHb. Second, within the VTA, the innervation pattern varied significantly from subregion to subregion.

Figure 3. Intersectional strategy for probing neurons co-expressing VGLUT1 and VGAT

(A) Triple transgenic breeding scheme for labeling neurons co-expressing VGLUT1 and VGAT.

(B) Distributions of labeled neurons in VGLUT1-Cre;VGAT-FlpO;Ai65 mice at different coronal planes.

(C) Representative images of tdTomato (tdT) labeling in the PIR and EPd (left), CA1 and DG (right).

(D–G) Co-injection of AAV9-DIO-EGFP/AAV9-fDIO-tdT in VGLUT1-Cre;VGAT-FlpO mice revealed no EGFP/tdT co-labeled neurons in the PIR (D), EPd (E), CA1 (F), and DG (G) in adults.

Scale bars: 200 μm (C), 50 μm (D–G).

Figure 4. VGLUT2 and VGAT co-expressing neurons probed with reporter line or intersectional AAV

(A) Triple transgenic breeding scheme for labeling neurons co-expressing VGLUT2 and VGAT.

(B) Distributions of labeled neurons in VGLUT2-Cre;VGAT-FlpO;Ai65 mice at different coronal planes.

(C) Representative images of tdT labeling in Ai65.

(D) Selective images of labeled axonal terminals in the LHb and DG.

Third, six regions (GPi, IF, RLi, CLi, SCs, MPT) innervated the LHb with either glutamate transmission or glutamate/GABA co-transmission, exclusive of GABA transmission. Fourth, other regions (PN, PBP, MEApd-a, LPO, posterior SI, MA, COA, EW) used all three types of transmission (glutamate transmission, GABA transmission, glutamate/GABA co-transmission), without a dominant type.

In addition to the 14 regions conducting glutamate/GABA co-transmission (Figure 5E), co-injection of AAV2-retro-DIO-EGFP/AAV2-retro-fDIO-tdTomato also revealed 23 LHb-projecting regions exclusive of VGLUT2/VGAT projecting neurons (Figure 6A). These regions provided glutamatergic innervations alone (six regions), GABAergic innervations alone (11 regions), or mixed innervations originated from sole glutamatergic and sole GABAergic neurons (six regions). Twelve regions (mPFC, LS, MS, NDB, BST, CEA, SCN, PVT, LHA, MRN, LGN, and IGL) (Figure S8) have been identified in previous studies (Hu et al., 2020), and the other 11 regions (AHN, VMH, ZI, RE, BLAa, MGN, NOT, OP, PPT, PAG, and ND) have not been reported (Figure 6).

Unlike the LHb, the DG received glutamatergic/GABAergic co-innervation from only a few brain regions. The SUM is a major source (Figure 5F), consistent with previous reports that glutamate/GABA co-releasing neurons in the SUM innervate granule cells and GABAergic interneurons in the DG (Hashimotodani et al., 2018; Soussi et al., 2010). Meanwhile, a subset of L2 neurons in the dorsal one-third of the lateral entorhinal cortex (ENTl) also innervated the DG with axonal terminals co-expressing VGLUT2/VGAT (Figure 5G). Retrograde labeling with AAV2-retro-DIO-EGFP/AAV2-retro-fDIO-tdTomato co-injection revealed that ~56% of the SUM projections and ~30% of the ENTl L2 projections from the dorsal one-third innervate the DG with glutamate/GABA co-transmission (Figure 5H).

VGlut3/VGAT intersections

In VGLUT3-Cre;VGAT-FlpO;Ai65 mice, tdTomato-labeled neurons were distributed in ~21 brain structures (Figures 7B and 7J). Most of these structures were located in the midbrain and thalamus, but the CA3, amygdala, and L6 of the isocortex also contained labeled neurons. Interestingly, a fraction of L6 neurons were positive for Pvalb antibody staining (data not shown), suggesting these neurons might be the same ones observed in the VGLUT3-Cre/Pvalb-FlpO intersection (Figures S3C and S4D).

AAV9-C$_{on}$/F$_{on}$-EYFP injection or AAV9-DIO-EGFP/AAV9-fDIO-tdTomato co-injection revealed that 11 structures, including CA3 (Figures 7D and 7E), VTA (PN, IF) and IPN (IPR, IPA, IPDL, IPC, IPI, IPL) (Figures 7F and 7I), MEApd-c (Figure 7H), and BST (Figure 7G) continued to co-express VGLUT3 and VGAT in the adult. Other regions were not labeled with AAV9-C$_{on}$/F$_{on}$-EYFP and only showed VGAT expression, but not VGLUT3 expression, with AAV9-DIO-EGFP/AAV9-fDIO-tdTomato co-injection. Thus, these regions may only express VGLUT3 transiently during development. The results are summarized in Figure 7J.

DISCUSSION

The past few years have seen the creation of increasing numbers of Flp and tTA driver lines, a trend that is expected to continue. A growing number of driver lines will increase the likelihood that many laboratories will adopt and exploit intersectional strategies in the future. Characterization of existing Cre, Flp, and tTA driver lines combined with transcriptome studies and protein expression profiling to generate new lines are prerequisites for widespread adoption. The intersectional mouse lines created and characterized here provide a common basis and useful resource for elucidating new cell types and circuits in the brain.

Glutamatergic neurons expressing GABAergic markers

Pvalb, SST, and VIP are prominent markers for GABAergic neurons in the cortex. To our surprise, we were able to find numerous glutamatergic neurons that express GABAergic markers either transiently or permanently. Pvalb was transiently expressed in a subset of L5 PT corticofugal neurons. In the subcortical regions, Pvalb-expressing glutamatergic neurons were discovered in nine structures. Except for the parvafox nucleus (Girard et al., 2011), functional studies of Pvalb-expressing glutamatergic neurons are largely lacking. A brain-wide knockout of VGLUT2 in Pvalb neurons led to several behavior changes, including locomotion, vocalization, pain sensitivity, and social dominance (Roccaro-Waldmeyer et al., 2018), suggesting important roles for Pvalb-expressing (or transiently expressing) glutamatergic neurons in various behaviors. Future studies targeting specific brain regions will deepen our understanding of the circuit and behavior roles of these neurons in each structure.
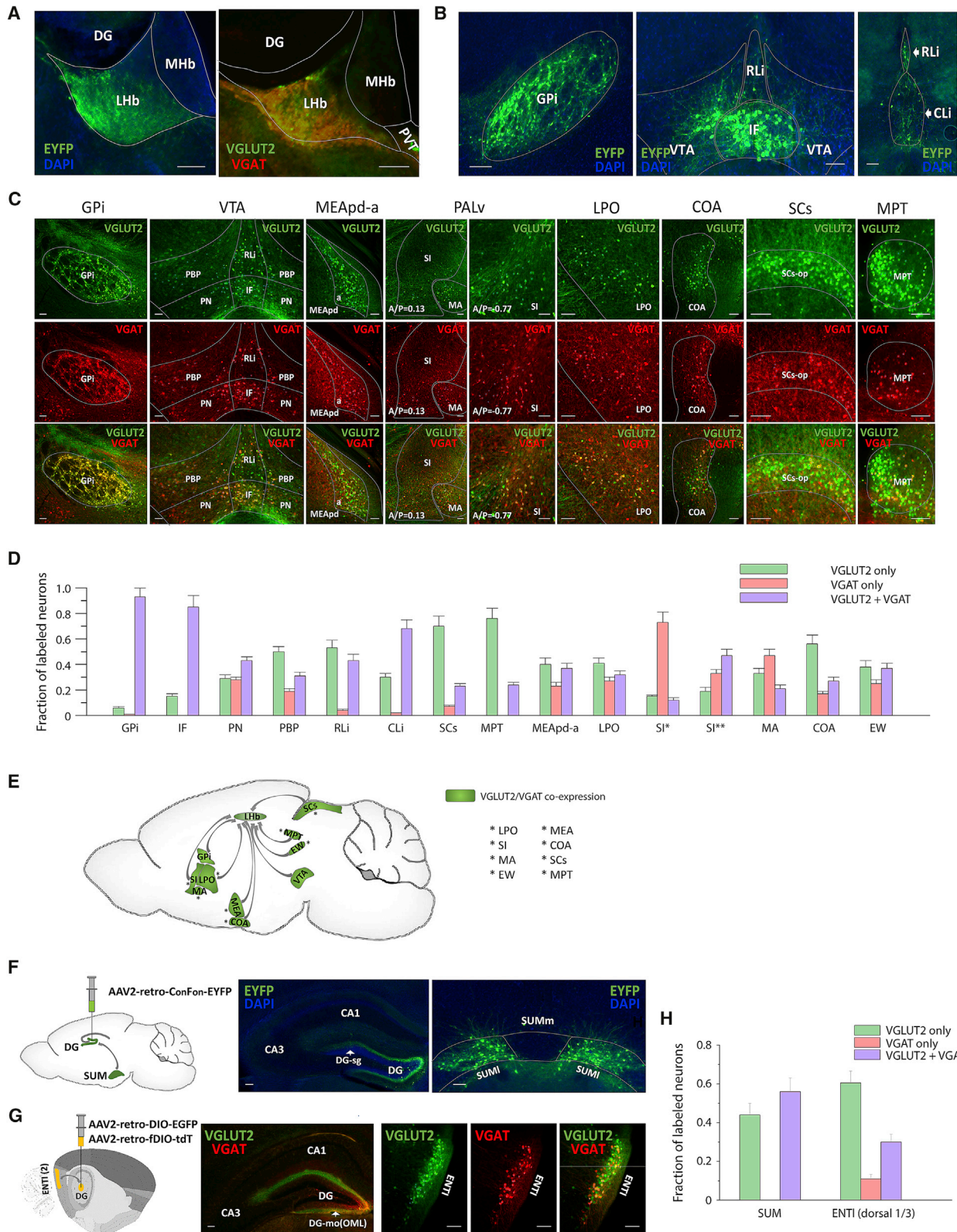
Neurotransmitter co-release during development

Neurons can change their neurotransmitter content dramatically during development stages, including switching from dual glutamate/GABA during development to either glutamate or GABA later in life (Spitzer, 2017). Coexistence of glutamate and GABA transmissions during development would allow a neuron to establish precisely organized circuit connectivity. For example, glutamate transmission is crucial for refinement of inhibitory circuits in the developing lateral superior olive (LSO), a nucleus of the sound-localization system (Gillespie et al., 2005; Noh et al., 2010). Interestingly, under some conditions, the "disappeared neurotransmitter" may come back later in life to correct disrupted balance of excitation and inhibition. For instance, during development, glutamate and GABA were produced in dentate gyrus granule cells and they were co-released from mossy fiber synapses. In the adult, GABAergic transmission disappeared but can be transiently re-installed after seizures to counteract hyperexcitability (Gutierrez, 2005; Gutierrez et al., 2003; Leinekugel et al., 1997; Romo-Parra et al., 2003). Our results suggest that transient co-expression of glutamate/GABA is more widespread than previously anticipated. Evidence of transient co-expression

---

(E) Expression of VGLUT2 mRNA (red) and VGAT mRNA (green) probed with *in situ* hybridization. VGLUT2/VGAT co-expressing neurons are marked with blue arrows.

(F) Summary of Ai65 reported regions containing (green) or not containing (red) VGLUT2/VGAT co-expressing neurons as revealed by AAV9-Con/Fon-EYFP. The VTA region includes the PBP, PN, IF, RLi, and CLi. *Regions that have not been reported by previous studies. Scale bars: 200 μm (C and D), 20 μm (E).

was observed in 32 brain regions, including four regions from VGLUT1/VGAT intersections, 18 regions from VGLUT2/VGAT intersections, and 10 regions from VGLUT3/VGAT intersections. In the current study, we were unable to trace the time of VGLUT and VGAT expression. In the future, replacing Cre and Flp drivers with Cre-ER (Feil et al., 1996; Metzger et al., 1995) and Flp-ER (Hunter et al., 2005) drivers would allow one to trace the expression of glutamate and GABA at each developmental stage and target specific time periods to investigate the functional implications of neurotransmitter co-expression.

Neurons co-expressing excitatory and inhibitory neurotransmitter transporters in adults

Our results show that most adult dual glutamatergic/GABAergic neurons are projection neurons that use VGLUT2, while the other neurons are likely to be interneurons expressing VGLUT3. In contrast, neurons expressing VGLUT1 are exclusive of VGAT. Altogether, we identified 19 regions containing VGLUT2/VGAT co-expressing neurons. Interestingly, except for five regions (SUM, ENTl, SCm, PAA, DR), all of these regions send VGLUT2/VGAT co-expressing axonal terminals to the LHb. Thus, the LHb appears to be a primary target for glutamatergic/GABAergic co-innervation in the brain. Second to the LHb, the dentate gyrus also receives substantial co-innervation from the SUM and ENTl. The brain regions receiving co-innervations from the SCm, PAA, and DR need to be determined in the future.

The function of co-innervation in the LHb is not completely understood. A disruption of the balance between glutamatergic and GABAergic inputs from GPi or VTA has been linked to depression, anxiety, and addiction (Li et al., 2011; Meye et al., 2016; Shabel et al., 2014; Yang et al., 2018). The LHb lacks GABAergic interneurons (Brinschwitz et al., 2010; Wallace et al., 2020), so GABA co-released with glutamate could provide a fast feed-forward inhibition of glutamatergic excitation without recruiting the typical disynaptic inhibition that involves inhibitory interneurons. In addition to the GPi and VTA, we discovered that eight more structures contained VGLUT2/VGAT neurons projecting to the LHb. Thus, co-innervation is used by more brain structures to communicate with the LHb than previously reported. Our mapping of LHb-projecting neurons (Figures 5E and 6A) largely agrees with previous work (Hu et al., 2020; Namboodiri et al., 2016) and adds 14 more regions (COA, MEA, EW, and 11 regions in Figure 6) to the category. The LHb appears to act as a hub to integrate different inputs of value representation, sensory, and experience information. Here, we discovered three more retino-recipient areas (OP, PPT, and NOT) along with the medial geniculate complex (MGN), the major auditory nucleus of the thalamus that innervates the LHb (Figures 6B and 6E). Therefore, the LHb appears to integrate even more sensory information than originally thought. A recent study described four transcriptionally different neuron subtypes in the LHb that are organized into anatomical subregions and project to distinct downstream targets (Wallace et al., 2020). It will be interesting to know how the axonal terminals from different brain areas are arranged in the LHb, perhaps contacting different cell types within this structure, and how the LHb decodes information carried by these axonal terminals and communicates with downstream targets. Addressing these questions will greatly advance our understanding of signal processing in the LHb.

VGLUT3/VGAT co-expression has been described in the CCK interneurons in hippocampal CA3, where the VGLUT3-mediated glutamate release can regulate GABAergic transmission onto CA1 principal cells through an autoreceptor pre-synaptic mechanism shifting the synaptic plasticity (Fasano et al., 2017; Pelkey et al., 2020). Here, we also observed VGLUT3/VGAT co-expression neurons in the VTA (PN, IF), IPN (IPR, IPA, IPDL, IPC, IPI, IPL), MEApd-c, and BST. These neurons are likely interneurons, although future experiments will be required for verification. Meanwhile, it is important to examine if indeed VGLUT3 mediates glutamate release in these neurons. Although challenging, technical advances in optical sensors for glutamate (Marvin et al., 2018) and GABA (Marvin et al., 2019) release may allow direct monitoring of glutamate/GABA co-release from these neurons. Intersectional mouse lines such as VGLUT3-Cre;VGAT-FlpO set the stage for a greater understanding of the roles of co-release in circuit, behavior, and diseases.

Limitations of the study

At the technical level, confining viral infections to the LHb and DG can be challenging. Spillover of AAV2-retro-C$_{on}$/F$_{on}$-EYFP or AAV2-retro-DIO-EGFP/AAV2-retro-fDIO-tdTomato to surrounding structures can cause contamination of the presented results. We verified injection sites and examined spillover with immunohistochemistry for each brain before data collection. We found that projection patterns from multiple brains were rather consistent

---

Figure 5. VGLUT2 and VGAT co-expressing neurons projecting to the LHb or DG

(A) LHb was injected with AAV2-retro-Con/Fon-EYFP (left), or AAV2-retro-DIO-EGFP/AAV2-retro-fDIO-tdT (right).

(B) Representative images of EYFP+ neurons labeled with AAV2-retro-Con/Fon-EYFP injected in the LHb.

(C) Representative images of neurons labeled with AAV2-retro-DIO-EGFP/AAV2-retro-fDIO-tdT co-injected in the LHb. Blue dots: neurons double positive for EGFP and tdTomato.

(D) Fractions of neurons innervating the LHb with sole glutamatergic transmission, sole GABAergic transmission, and glutamatergic/GABAergic co-transmission in different projecting areas. *A/p = 0.13 mm, **A/p = −0.77 mm. n = 5 brains, data are presented as mean ± SEM. See also Table S5 for more information.

(E) Summary of LHb-projecting regions sending VGLUT2/VGAT co-expressing axonal terminals. The VTA includes the PBP, PN, IF, RLi, and CLi. *Regions that have not been reported by previous studies.

(F and G) Retrograde labeling of SUM-projecting neurons (F) and ENTl-projecting neurons (G) co-expressing VGLUT2/VGAT from the DG. Blue dots in (G): neurons co-labeled with EGFP and tdTomato.

(H) Fractions of neurons innervating the DG with sole glutamatergic transmission, sole GABAergic transmission, and glutamatergic/GABAergic co-transmission in the SUM and ENTl (dorsal 1/3), as determined by AAV2-retro-DIO-EGFP/AAV2-retro-fDIO-tdT co-injection in the DG. n = 6 brains, data are presented as mean ± SEM. Experiments were performed on VGLUT2-Cre;VGAT-FlpO mice.

Scale bars: 100 μm (A, C, F, and G), 200 μm (B).
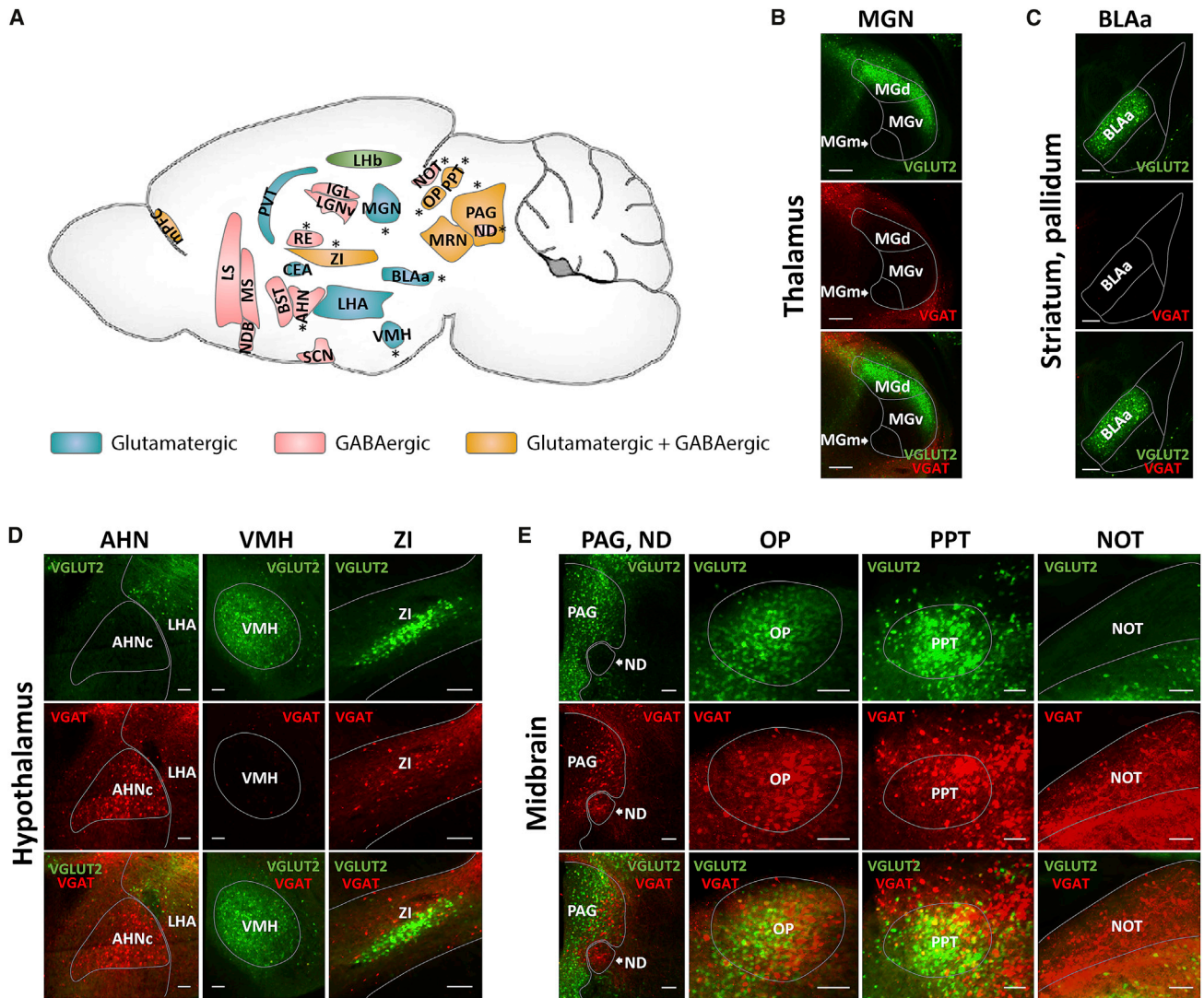
Figure 6. LHb-projecting regions excluding VGLUT2/VGAT co-expressing axonal terminals

(A) Summary of LHb-projecting regions providing glutamatergic innervations alone (blue), GABAergic innervations alone (pink), or mixed innervations originated from sole glutamatergic and sole GABAergic neurons (orange). *Regions that have not been reported by previous studies.

(B–E) Representative images of labeled structures that have not been reported by previous studies. See Figure S8 for regions that have been reported. Experiments were performed on VGLUT2-Cre;VGAT-FlpO mice with AAV2-retro-DIO-EGFP/AAV2-retro-fDIO-tdT mix injected into the LHb.

Scale bars: 200 μm (B and C), 100 μm (D and E).

with each other. However, we cannot completely rule out the possibility that weak off-target infections occurred but were not detected under our analysis. Future functional studies such as ChR2 and/or electrophysiological recordings need to be performed to validate the projections discovered in this study, along with the neurotransmitters used for these transmissions. Meanwhile, the strengths of glutamatergic and GABAergic projections from the VGLUT2/VGAT co-expressing neurons have not been accessed in this study. It is important to determine whether the two projections are well balanced or one projection dominates the other. Finally, the viral infection was not restricted to the subregions within the LHb or the DG. As projection patterns to the LHb or the DG can vary significantly from subregion to subregion,
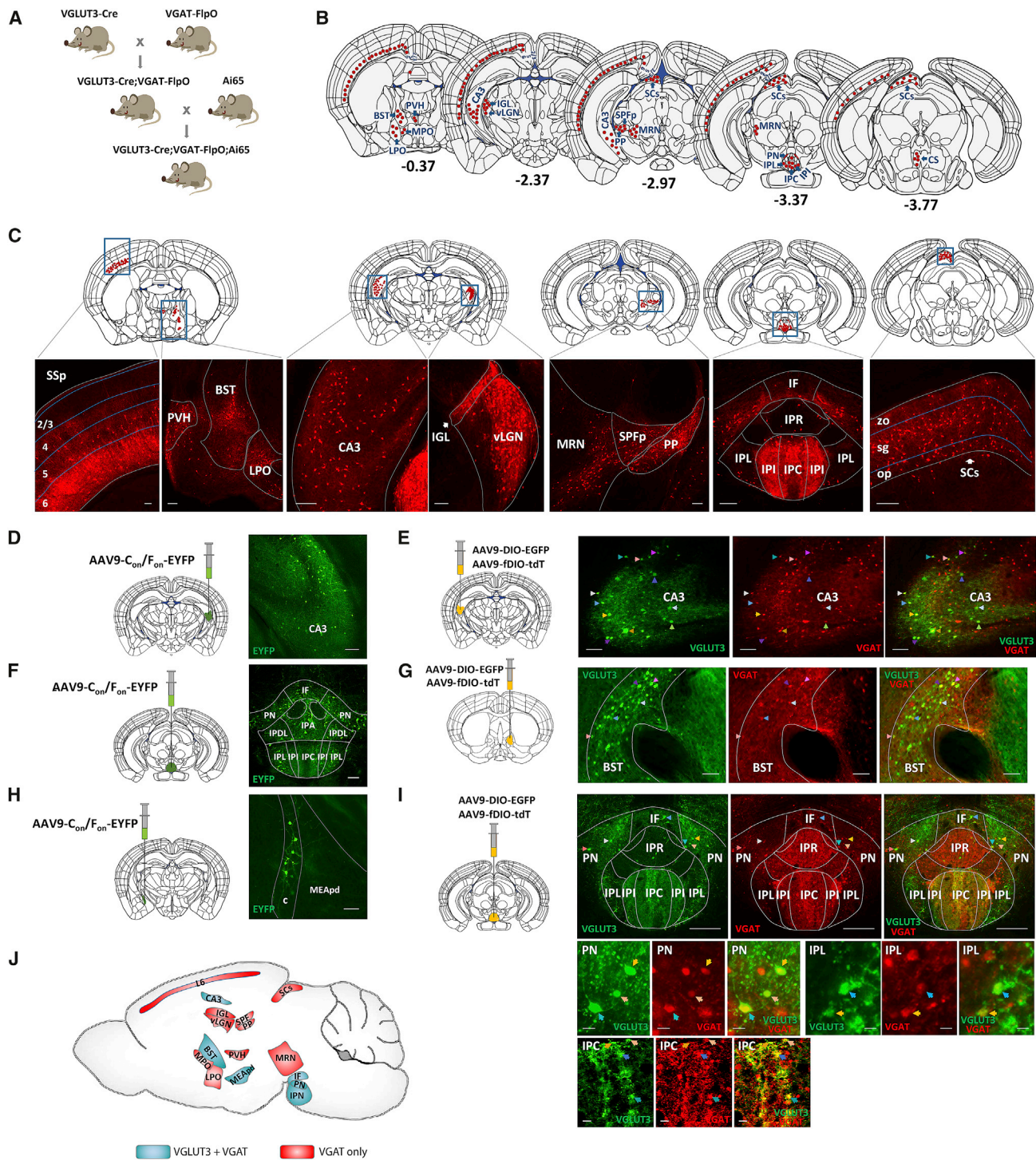
future studies should be directed to expand this work to a subregional level.

STAR★METHODS

Detailed methods are provided in the online version of this paper and include the following:

- KEY RESOURCES TABLE
- RESOURCE AVAILABILITY
  - ○ Lead contact
  - ○ Materials availability
  - ○ Data and code availability

Figure 7. VGLUT3 and VGAT co-expressing neurons in the brain

(A) Triple transgenic breeding scheme for labeling neurons co-expressing VGlut3 and VGAT.

(B) Distributions of labeled neurons in VGLUT3-Cre;VGAT-FlpO;Ai65 mice at different coronal planes.

(C) Representative images of tdT labeling in VGLUT3-Cre;VGAT-FlpO;Ai65 mice.

(D–I) Intersectional AAVs confirmed VGLUT3/VGAT co-expression in neurons of the CA3 (D, E), IF (F, I), PN (F, I), IPN (F, I), MEApd-c (H), and BST (G). Experiments were performed in VGLUT3-Cre;VGAT-FlpO mice.

(J) Summary of Ai65 reported regions that contain VGLUT3/VGAT co-expressing neurons (blue) and regions that only contain VGAT-expressing neurons (red).

Scale bars: 100 μm (C–I, top), 20 μm (I, middle, bottom).

- ● EXPERIMENTAL MODEL AND SUBJECT DETAILS
  - ○ Animal care and use
  - ○ HEK 293T cells culture
- ● METHOD DETAILS
  - ○ Molecular cloning
  - ○ Viral packaging and titering
  - ○ Stereotaxic injections
  - ○ Immunohistochemistry and imaging
  - ○ In situ Hybridization/RNAscope
- ● QUANTIFICATION AND STATISTICAL ANALYSIS

REFERENCES

Boulland, J.L., Qureshi, T., Seal, R.P., Rafiki, A., Gundersen, V., Bergersen, L.H., Fremeau, R.T., Jr., Edwards, R.H., Storm-Mathisen, J., and Chaudhry, F.A. (2004). Expression of the vesicular glutamate transporters during development indicates the widespread corelease of multiple neurotransmitters. J. Comp. Neurol. *480*, 264–280. https://doi.org/10.1002/cne.20354.

Brinschwitz, K., Dittgen, A., Madai, V.I., Lommel, R., Geisler, S., and Veh, R.W. (2010). Glutamatergic axons from the lateral habenula mainly terminate on GABAergic neurons of the ventral midbrain. Neuroscience *168*, 463–476. https://doi.org/10.1016/j.neuroscience.2010.03.050.

Broach, J.R., Guarascio, V.R., and Jayaram, M. (1982). Recombination within the yeast plasmid 2µ circle is site-specific. Cell *29*, 227–234. https://doi.org/10.1016/0092-8674(82)90107-6.

Cowan, C.S., Renner, M., De Gennaro, M., Gross-Scherf, B., Goldblum, D., Hou, Y., Munz, M., Rodrigues, T.M., Krol, J., Szikra, T., et al. (2020). Cell types of the human retina and its organoids at single-cell resolution. Cell *182*, 1623–1640.e34. https://doi.org/10.1016/j.cell.2020.08.013.

Daigle, T.L., Madisen, L., Hage, T.A., Valley, M.T., Knoblich, U., Larsen, R.S., Takeno, M.M., Huang, L., Gu, H., Larsen, R., et al. (2018). A suite of transgenic driver and reporter mouse lines with enhanced brain-cell-type targeting and functionality. Cell *174*, 465–480.e22. https://doi.org/10.1016/j.cell.2018.06.035.

Dymecki, S.M., Ray, R.S., and Kim, J.C. (2010). Mapping cell fate and function using recombinase-based intersectional strategies. Methods Enzymol. *477*, 183–213. https://doi.org/10.1016/S0076-6879(10)77011-7.

Fasano, C., Rocchetti, J., Pietrajtis, K., Zander, J.F., Manseau, F., Sakae, D.Y., Marcus-Sells, M., Ramet, L., Morel, L.J., Carrel, D., et al. (2017). Regulation of the hippocampal network by VGLUT3-positive CCK- GABAergic basket cells. Front. Cell. Neurosci. *11*, 140. https://doi.org/10.3389/fncel.2017.00140.

Feil, R., Brocard, J., Mascrez, B., LeMeur, M., Metzger, D., and Chambon, P. (1996). Ligand-activated site-specific recombination in mice. Proc. Natl. Acad. Sci. USA *93*, 10887–10890. https://doi.org/10.1073/pnas.93.20.10887.

Fenno, L.E., Mattis, J., Ramakrishnan, C., Hyun, M., Lee, S.Y., He, M., Tucciarone, J., Selimbeyoglu, A., Berndt, A., Grosenick, L., et al. (2014). Targeting cells with single vectors using multiple-feature Boolean logic. Nat. Methods *11*, 763–772. https://doi.org/10.1038/nmeth.2996.

Fenno, L.E., Ramakrishnan, C., Kim, Y.S., Evans, K.E., Lo, M., Vesuna, S., Inoue, M., Cheung, K.Y.M., Yuen, E., Pichamoorthy, N., et al. (2020). Comprehensive dual- and triple-feature intersectional single-vector delivery of diverse functional payloads to cells of behaving mammals. Neuron *107*, 836–853.e11. https://doi.org/10.1016/j.neuron.2020.06.003.

Fremeau, R.T., Jr., Voglmaier, S., Seal, R.P., and Edwards, R.H. (2004). VGLUTs define subsets of excitatory neurons and suggest novel roles for glutamate. Trends Neurosci. *27*, 98–103. https://doi.org/10.1016/j.tins.2003.11.005.

Gillespie, D.C., Kim, G., and Kandler, K. (2005). Inhibitory synapses in the developing auditory system are glutamatergic. Nat. Neurosci. *8*, 332–338. https://doi.org/10.1038/nn1397.

Girard, F., Meszar, Z., Marti, C., Davis, F.P., and Celio, M. (2011). Gene expression analysis in the parvalbumin-immunoreactive PV1 nucleus of the mouse lateral hypothalamus. Eur. J. Neurosci. *34*, 1934–1943. https://doi.org/10.1111/j.1460-9568.2011.07918.x.

Gossen, M., and Bujard, H. (1992). Tight control of gene expression in mammalian cells by tetracycline-responsive promoters. Proc. Natl. Acad. Sci. USA *89*, 5547–5551. https://doi.org/10.1073/pnas.89.12.5547.

Granger, A.J., Wallace, M.L., and Sabatini, B.L. (2017). Multi-transmitter neurons in the mammalian central nervous system. Curr. Opin. Neurobiol. *45*, 85–91. https://doi.org/10.1016/j.conb.2017.04.007.

Gray, S.J., Choi, V.W., Asokan, A., Haberman, R.A., McCown, T.J., and Samulski, R.J. (2011). Production of recombinant adeno-associated viral vectors and use in *in vitro* and *in vivo* administration. Curr. Protoc. Neurosci. Chapter 4, Unit 4.17. https://doi.org/10.1002/0471142301.ns0417s57.

Gutiérrez, R. (2005). The dual glutamatergic-GABAergic phenotype of hippocampal granule cells. Trends Neurosci. *28*, 297–303. https://doi.org/10.1016/j.tins.2005.04.005.

Gutiérrez, R., Romo-Parra, H., Maqueda, J., Vivar, C., Ramìrez, M., Morales, M.A., and Lamas, M. (2003). Plasticity of the GABAergic phenotype of the "glutamatergic" granule cells of the rat dentate gyrus. J. Neurosci. *23*, 5594–5598. https://doi.org/10.1523/jneurosci.23-13-05594.2003.

Hashimotodani, Y., Karube, F., Yanagawa, Y., Fujiyama, F., and Kano, M. (2018). Supramammillary nucleus afferents to the dentate gyrus Co-release glutamate and GABA and potentiate granule cell output. Cell Rep. *25*, 2704–2715.e4. https://doi.org/10.1016/j.celrep.2018.11.016.

Hawrylycz, M., Bernard, A., Lau, C., Sunkin, S.M., Chakravarty, M.M., Lein, E.S., Jones, A.R., and Ng, L. (2010). Areal and laminar differentiation in the

mouse neocortex using large scale gene expression data. Methods *50*, 113–121. https://doi.org/10.1016/j.ymeth.2009.09.005.

He, M., Tucciarone, J., Lee, S., Nigro, M.J., Kim, Y., Levine, J.M., Kelly, S.M., Krugikov, I., Wu, P., Chen, Y., et al. (2016). Strategies and tools for combinatorial targeting of GABAergic neurons in mouse cerebral cortex. Neuron *91*, 1228–1243. https://doi.org/10.1016/j.neuron.2016.08.021.

Hodge, R.D., Bakken, T.E., Miller, J.A., Smith, K.A., Barkan, E.R., Graybuck, L.T., Close, J.L., Long, B., Johansen, N., Penn, O., et al. (2019). Conserved cell types with divergent features in human versus mouse cortex. Nature *573*, 61–68. https://doi.org/10.1038/s41586-019-1506-7.

Hu, H., Cui, Y., and Yang, Y. (2020). Circuits and functions of the lateral habenula in health and in disease. Nat. Rev. Neurosci. *21*, 277–295. https://doi.org/10.1038/s41583-020-0292-4.

Huang, K.W., Ochandarena, N.E., Philson, A.C., Hyun, M., Birnbaum, J.E., Cicconet, M., and Sabatini, B.L. (2019). Molecular and anatomical organization of the dorsal raphe nucleus. Elife *8*, e46464. https://doi.org/10.7554/elife.46464.

Hunter, N.L., Awatramani, R.B., Farley, F.W., and Dymecki, S.M. (2005). Ligand-activated Flpe for temporally regulated gene modifications. Genesis *41*, 99–109. https://doi.org/10.1002/gene.20101.

Jo, A., Xu, J., Deniz, S., Cherian, S., DeVries, S.H., and Zhu, Y. (2018). Intersectional strategies for targeting amacrine and ganglion cell types in the mouse retina. Front. Neural Circuits *12*, 66. https://doi.org/10.3389/fncir.2018.00066.

Kim, E.J., Zhang, Z., Huang, L., Ito-Cole, T., Jacobs, M.W., Juavinett, A.L., Senturk, G., Hu, M., Ku, M., Ecker, J.R., and Callaway, E.M. (2020). Extraction of distinct neuronal cell types from within a genetically continuous population. Neuron *107*, 274–282.e6. https://doi.org/10.1016/j.neuron.2020.04.018.

Kim, Y., Yang, G.R., Pradhan, K., Venkataraju, K.U., Bota, M., García del Molino, L.C., Fitzgerald, G., Ram, K., He, M., Levine, J.M., et al. (2017). Brain-wide maps reveal stereotyped cell-type-based cortical architecture and subcortical sexual dimorphism. Cell *171*, 456–469.e22. https://doi.org/10.1016/j.cell.2017.09.020.

Lein, E.S., Hawrylycz, M.J., Ao, N., Ayres, M., Bensinger, A., Bernard, A., Boe, A.F., Boguski, M.S., Brockway, K.S., Byrnes, E.J., et al. (2007). Genome-wide atlas of gene expression in the adult mouse brain. Nature *445*, 168–176. https://doi.org/10.1038/nature05453.

Leinekugel, X., Medina, I., Khalilov, I., Ben-Ari, Y., and Khazipov, R. (1997). Ca2+ oscillations mediated by the synergistic excitatory actions of GABA(A) and NMDA receptors in the neonatal hippocampus. Neuron *18*, 243–255. https://doi.org/10.1016/s0896-6273(00)80265-2.

Li, B., Piriz, J., Mirrione, M., Chung, C., Proulx, C.D., Schulz, D., Henn, F., and Malinow, R. (2011). Synaptic potentiation onto habenula neurons in the learned helplessness model of depression. Nature *470*, 535–539. https://doi.org/10.1038/nature09742.

Madisen, L., Garner, A.R., Shimaoka, D., Chuong, A.S., Klapoetke, N.C., Li, L., van der Bourg, A., Niino, Y., Egolf, L., Monetti, C., et al. (2015). Transgenic mice for intersectional targeting of neural sensors and effectors with high specificity and performance. Neuron *85*, 942–958. https://doi.org/10.1016/j.neuron.2015.02.022.

Martersteck, E.M., Hirokawa, K.E., Evarts, M., Bernard, A., Duan, X., Li, Y., Ng, L., Oh, S.W., Ouellette, B., Royall, J.J., et al. (2017). Diverse central projection patterns of retinal ganglion cells. Cell Rep. *18*, 2058–2072. https://doi.org/10.1016/j.celrep.2017.01.075.

Marvin, J.S., Scholl, B., Wilson, D.E., Podgorski, K., Kazemipour, A., Müller, J.A., Schoch, S., Quiroz, F.J.U., Rebola, N., Bao, H., et al. (2018). Stability, affinity, and chromatic variants of the glutamate sensor iGluSnFR. Nat. Methods *15*, 936–939. https://doi.org/10.1038/s41592-018-0171-3.

Marvin, J.S., Shimoda, Y., Magloire, V., Leite, M., Kawashima, T., Jensen, T.P., Kolb, I., Knott, E.L., Novak, O., Podgorski, K., et al. (2019). A genetically encoded fluorescent sensor for *in vivo* imaging of GABA. Nat. Methods *16*, 763–770. https://doi.org/10.1038/s41592-019-0471-2.

Metzger, D., Clifford, J., Chiba, H., and Chambon, P. (1995). Conditional site-specific recombination in mammalian cells using a ligand-dependent chimeric Cre recombinase. Proc. Natl. Acad. Sci. USA *92*, 6991–6995. https://doi.org/10.1073/pnas.92.15.6991.

Meye, F.J., Soiza-Reilly, M., Smit, T., Diana, M.A., Schwarz, M.K., and Mameli, M. (2016). Shifted pallidal co-release of GABA and glutamate in habenula drives cocaine withdrawal and relapse. Nat. Neurosci. *19*, 1019–1024. https://doi.org/10.1038/nn.4334.

Namboodiri, V.M.K., Rodriguez-Romaguera, J., and Stuber, G.D. (2016). The habenula. Curr. Biol. *26*, R873–R877. https://doi.org/10.1016/j.cub.2016.08.051.

Noh, J., Seal, R.P., Garver, J.A., Edwards, R.H., and Kandler, K. (2010). Glutamate co-release at GABA/glycinergic synapses is crucial for the refinement of an inhibitory map. Nat. Neurosci. *13*, 232–238. https://doi.org/10.1038/nn.2478.

Paxinos, G., and Franklin, K.B.J. (2004). The mouse brain in stereotaxic coordinates. Compact, 2nd ed. (Boston: Amsterdam).

Pedersen, N.P., Ferrari, L., Venner, A., Wang, J.L., Abbott, S.B.G., Vujovic, N., Arrigoni, E., Saper, C.B., and Fuller, P.M. (2017). Supramammillary glutamate neurons are a key node of the arousal system. Nat. Commun. *8*, 1405. https://doi.org/10.1038/s41467-017-01004-6.

Pelkey, K.A., Calvigioni, D., Fang, C., Vargish, G., Ekins, T., Auville, K., Wester, J.C., Lai, M., Mackenzie-Gray Scott, C., Yuan, X., et al. (2020). Paradoxical network excitation by glutamate release from VGluT3(+) GABAergic interneurons. Elife *9*, e51996. https://doi.org/10.7554/elife.51996.

Peng, Y.R., Shekhar, K., Yan, W., Herrmann, D., Sappington, A., Bryman, G.S., van Zyl, T., Do, M.T.H., Regev, A., and Sanes, J.R. (2019). Molecular classification and comparative taxonomics of foveal and peripheral cells in primate retina. Cell *176*, 1222–1237.e22. https://doi.org/10.1016/j.cell.2019.01.004.

Poulin, J.-F., Caronia, G., Hofer, C., Cui, Q., Helm, B., Ramakrishnan, C., Chan, C.S., Dombeck, D.A., Deisseroth, K., and Awatramani, R. (2018). Mapping projections of molecularly defined dopamine neuron subtypes using intersectional genetic approaches. Nat. Neurosci. *21*, 1260–1271. https://doi.org/10.1038/s41593-018-0203-4.

Ren, J., Isakova, A., Friedmann, D., Zeng, J., Grutzner, S.M., Pun, A., Zhao, G.Q., Kolluru, S.S., Wang, R., Lin, R., et al. (2019). Single-cell transcriptomes and whole-brain projections of serotonin neurons in the mouse dorsal and median raphe nuclei. Elife *8*, e49424. https://doi.org/10.7554/elife.49424.

Roccaro-Waldmeyer, D.M., Girard, F., Milani, D., Vannoni, E., Prétôt, L., Wolfer, D.P., and Celio, M.R. (2018). Eliminating the VGlut2-dependent glutamatergic transmission of parvalbumin-expressing neurons leads to deficits in locomotion and vocalization, decreased pain sensitivity, and increased dominance. Front. Behav. Neurosci. *12*, 146. https://doi.org/10.3389/fnbeh.2018.00146.

Romo-Parra, H., Vivar, C., Maqueda, J., Morales, M.A., and Gutiérrez, R. (2003). Activity-dependent induction of multitransmitter signaling onto pyramidal cells and interneurons of hippocampal area CA3. J. Neurophysiol. *89*, 3155–3167. https://doi.org/10.1152/jn.00985.2002.

Root, D.H., Mejias-Aponte, C.A., Zhang, S., Wang, H.L., Hoffman, A.F., Lupica, C.R., and Morales, M. (2014). Single rodent mesohabenular axons release glutamate and GABA. Nat. Neurosci. *17*, 1543–1551. https://doi.org/10.1038/nn.3823.

Root, D.H., Zhang, S., Barker, D.J., Miranda-Barrientos, J., Liu, B., Wang, H.L., and Morales, M. (2018). Selective brain distribution and distinctive synaptic architecture of dual glutamatergic-GABAergic neurons. Cell Rep. *23*, 3465–3479. https://doi.org/10.1016/j.celrep.2018.05.063.

Shabel, S.J., Proulx, C.D., Piriz, J., and Malinow, R. (2014). Mood regulation. GABA/glutamate co-release controls habenula output and is modified by antidepressant treatment. Science *345*, 1494–1498. https://doi.org/10.1126/science.1250469.

Sonoda, T., Li, J.Y., Hayes, N.W., Chan, J.C., Okabe, Y., Belin, S., Nawabi, H., and Schmidt, T.M. (2020). A noncanonical inhibitory circuit dampens behavioral sensitivity to light. Science *368*, 527–531. https://doi.org/10.1126/science.aay3152.

Soussi, R., Zhang, N., Tahtakran, S., Houser, C.R., and Esclapez, M. (2010). Heterogeneity of the supramammillary-hippocampal pathways: evidence for a unique GABAergic neurotransmitter phenotype and regional differences. Eur. J. Neurosci. *32*, 771–785. https://doi.org/10.1111/j.1460-9568.2010.07329.x.

Spitzer, N.C. (2017). Neurotransmitter switching in the developing and adult brain. Annu. Rev. Neurosci. *40*, 1–19. https://doi.org/10.1146/annurev-neuro-072116-031204.

Taniguchi, H., He, M., Wu, P., Kim, S., Paik, R., Sugino, K., Kvitsani, D., Fu, Y., Lu, J., Lin, Y., et al. (2011). A resource of Cre driver lines for genetic targeting of GABAergic neurons in cerebral cortex. Neuron *71*, 995–1013. https://doi.org/10.1016/j.neuron.2011.07.026.

Tasic, B., Menon, V., Nguyen, T.N., Kim, T.K., Jarsky, T., Yao, Z., Levi, B., Gray, L.T., Sorensen, S.A., Dolbeare, T., et al. (2016). Adult mouse cortical cell taxonomy revealed by single cell transcriptomics. Nat. Neurosci. *19*, 335–346. https://doi.org/10.1038/nn.4216.

Tasic, B., Yao, Z., Graybuck, L.T., Smith, K.A., Nguyen, T.N., Bertagnolli, D., Goldy, J., Garren, E., Economo, M.N., Viswanathan, S., et al. (2018). Shared and distinct transcriptomic cell types across neocortical areas. Nature *563*, 72–78. https://doi.org/10.1038/s41586-018-0654-5.

Tritsch, N.X., Granger, A.J., and Sabatini, B.L. (2016). Mechanisms and functions of GABA co-release. Nat. Rev. Neurosci. *17*, 139–145. https://doi.org/10.1038/nrn.2015.21.

Wallace, M.L., Huang, K.W., Hochbaum, D., Hyun, M., Radeljic, G., and Sabatini, B.L. (2020). Anatomical and single-cell transcriptional profiling of the murine habenular complex. Elife *9*, e51271. https://doi.org/10.7554/elife.51271.

Wallace, M.L., Saunders, A., Huang, K.W., Philson, A.C., Goldman, M., Macosko, E.Z., McCarroll, S.A., and Sabatini, B.L. (2017). Genetically distinct parallel pathways in the entopeduncular nucleus for limbic and sensorimotor output of the basal ganglia. Neuron *94*, 138–152.e5. https://doi.org/10.1016/j.neuron.2017.03.017.

Xu, J., DeVries, S.H., and Zhu, Y. (2020). Quantification of adeno-associated virus with safe nucleic acid dyes. Hum. Gene Ther. *31*, 1086–1099. https://doi.org/10.1089/hum.2020.063.

Yang, B., Sanches-Padilla, J., Kondapalli, J., Morison, S.L., Delpire, E., Awatramani, R., and Surmeier, D.J. (2021). Locus coeruleus anchors a trisynaptic circuit controlling fear-induced suppression of feeding. Neuron *109*, 823–838.e6. https://doi.org/10.1016/j.neuron.2020.12.023.

Yang, Y., Wang, H., Hu, J., and Hu, H. (2018). Lateral habenula in the pathophysiology of depression. Curr. Opin. Neurobiol. *48*, 90–96. https://doi.org/10.1016/j.conb.2017.10.024.

Yao, Z., van Velthoven, C.T.J., Nguyen, T.N., Goldy, J., Sedeno-Cortes, A.E., Baftizadeh, F., Bertagnolli, D., Casper, T., Chiang, M., Crichton, K., et al. (2021). A taxonomy of transcriptomic cell types across the isocortex and hippocampal formation. Cell *184*, 3222–3241.

Yoo, J.H., Zell, V., Gutierrez-Reed, N., Wu, J., Ressler, R., Shenasa, M.A., Johnson, A.B., Fife, K.H., Faget, L., and Hnasko, T.S. (2016). Ventral tegmental area glutamate neurons co-release GABA and promote positive reinforcement. Nat. Commun. *7*, 13697. https://doi.org/10.1038/ncomms13697.

Yuste, R., Hawrylycz, M., Aalling, N., Aguilar-Valles, A., Arendt, D., Armañanzas, R., Ascoli, G.A., Bielza, C., Bokharaie, V., Bergmann, T.B., et al. (2020). A community-based transcriptomics classification and nomenclature of neocortical cell types. Nat. Neurosci. *23*, 1456–1468. https://doi.org/10.1038/s41593-020-0685-8.

Zhu, Y., Xu, J., Hauswirth, W.W., and DeVries, S.H. (2014). Genetically targeted binary labeling of retinal neurons. J. Neurosci. *34*, 7845–7861. https://doi.org/10.1523/jneurosci.2960-13.2014.

Zhuang, J., Ng, L., Williams, D., Valley, M., Li, Y., Garrett, M., and Waters, J. (2017). An extended retinotopic map of mouse cortex. Elife *6*, e18372. https://doi.org/10.7554/elife.18372.

Zolotukhin, S., Byrne, B.J., Mason, E., Zolotukhin, I., Potter, M., Chesnut, K., Summerford, C., Samulski, R.J., and Muzyczka, N. (1999). Recombinant adeno-associated virus purification using novel methods improves infectious titer and yield. Gene Ther. *6*, 973–985. https://doi.org/10.1038/sj.gt.3300938.

STAR★METHODS

KEY RESOURCES TABLE

REAGENT or RESOURCE	SOURCE	IDENTIFIER
Antibodies		
Goat anti-GFP	Abcam	ab5450; RRID:AB_304897
Rabbit anti-RFP	Rockland	600-401-379; RRID:AB_2209751
Mouse anti-parvalbumin	Swant	PV235; RRID:AB_10000343
Rat anti-SST	Millipore	MAB354; RRID:AB_2255365
Rabbit anti-VIP	ImmunoStar	20077; RRID:AB_572270
Alexa Fluor 488 donkey anti-goat IgG	Jackson Immunoresearch	705-545-003; RRID:AB_2340428
Alexa Fluor 488 donkey anti-mouse IgG	Jackson Immunoresearch	715-545-150; RRID:AB_2340846
Alexa Fluor 488 donkey anti-rat IgG	Jackson Immunoresearch	712-545-150;RRID:AB_2340683
Alexa Fluor 488 donkey anti-rabbit IgG	Jackson Immunoresearch	711-545-152; RRID:AB_2313584
Cy3 donkey anti-rabbit IgG	Jackson Immunoresearch	711-165-152; RRID:AB_2307443
Bacterial and virus strains		
pAAV-hSyn-Con/Fon-EYFP-WPRE	Fenno et al., 2014	Addgene: 55650
pAAV-Ef1a-fDIO- EYFP-WPRE	Fenno et al., 2014	Addgene: 55641
pAAV-CBA-Con/Fon-EYFP-WPRE	This study	Addgene: 186752
pAAV-Ef1a-DIO-EGFP -WPRE	This study	Addgene: 187103
pAAV-Ef1a-fDIO- tdTomato-WPRE	This study	Addgene: 187112
AAV9-CBA-Con/Fon-EYFP-WPRE	This study	N/A
AAV9-EF1a-DIO-EGFP-WPRE	This study	N/A
AAV9-EF1a-fDIO-tdTomato-WPRE	This study	N/A
AAV2-retro-CBA-Con/Fon-EYFP-WPRE	This study	N/A
AAV2-retro-EF1a-DIO-EGFP-WPRE	This study	N/A
AAV2-retro-EF1a-fDIO-tdTomato-WPRE	This study	N/A
Cell lines		
HEK 293T/17	ATCC	CRL-11268
Chemicals, peptides, and recombinant proteins		
DMEM	Corning	10-013-CM
Fetal bovine serum	Corning	35-011-CV
Penicillin-Streptomycin (100x)	Gibco	15140122
Trypsin-EDTA	Gibco	25300-054
Deposited data		
Allen Mouse Brain Reference Atlas	Allen Institute	https://mouse.brain-map.org/static/atlas
Allen Mouse Brain *in situ* hybridization Atlas	Allen Institute	https://mouse.brain-map.org/
Allen Mouse Brain Connectivity Atlas/ Transgenic Characterization	Allen Institute	http://connectivity.brain-map.org/transgenic
Experimental models: Organisms/strains		
Mouse: Ccktm1:1.cre/Zjh/J CCK-Cre	The Jackson Laboratory	JAX: 012706
Mouse: B6.CTg(CMVcre)1Cgn/J CMV-Cre	The Jackson Laboratory	JAX: 006054
Mouse: B6(Cg)-CrhTM1.cre/Zjh/J CRH-Cre	The Jackson Laboratory	JAX: 012704
Mouse: B6.129-Tg(Pcp2-cre)2Mpin/J L7-Cre	The Jackson Laboratory	JAX: 004146

(Continued on next page)

Continued

REAGENT or RESOURCE	SOURCE	IDENTIFIER
Mouse: B6;129SPenktm2.cre/Hze/J Penk-Cre	The Jackson Laboratory	JAX: 025112
Mouse: B6;129P2-*Pvalb*$^{tm1(cre)Arbr}$/J Pvalb-Cre	The Jackson Laboratory	JAX: 008069
Mouse: B6;C3-Tg(Scnn1a-cre)3Aibs/J Scnn1a-Cre	The Jackson Laboratory	JAX: 009613
Mouse: Sst tm2.1(cre)Zjh/J SST-Cre	The Jackson Laboratory	JAX: 013044
Mouse: B6;129S-Slc17a7$^{tm1.1(cre)Hze}$/J VGLUT1-Cre	The Jackson Laboratory	JAX: 023527
Mouse: Slc17a6tm2.cre/Lowl/J VGLUT2-Cre	The Jackson Laboratory	JAX: 016963
Mouse: B6;129S-Slc17a8$^{tm1.1(cre)Hze}$/J VGLUT3-Cre	The Jackson Laboratory	JAX: 028534
Mouse: Slc32a1tm2.cre/Lowl/J VGAT-Cre	The Jackson Laboratory	JAX: 016962
Mouse: B6;129S-*Tac1*$^{tm1.1(cre)Hze}$/J Tac1-Cre	The Jackson Laboratory	JAX: 021877
Mouse: Tg(ml56iflpe)39Fsh/J Dlx5/6-FlpE	The Jackson Laboratory	JAX: 010815
Mouse: Nkx2-1tm2:1.flpo/Zjh/J Nkx2-FlpO	The Jackson Laboratory	JAX: 028577
Mouse: B6.Cg-Pvalbtm2:1.FLPe/Hze/J Pvalb-FlpE	The Jackson Laboratory	JAX: 021191
Mouse: B6.Cg-Rasgrf2$^{tm2.1(folA/flpo)Hze}$/J Rasgrf2-FlpO	The Jackson Laboratory	JAX: 029589
Mouse: B6.Cg-RorbTM3:1.flpo/Hze/J Rorb-FlpO	The Jackson Laboratory	JAX: 029590
Mouse: Ssttm3:1.flpo/Zjh/J SST-FlpO	The Jackson Laboratory	JAX: 028579
Mouse: VipTM2:1.flpo/Zjh/J VIP-FlpO	The Jackson Laboratory	JAX: 028578
Mouse: B6.Cg-Slc32a1TM1:1.flpo/Hze/J VGAT-FlpO	The Jackson Laboratory, Hongkui Zeng	JAX: 029591
Mouse: B6.Cg-Tg(Camk2a tTA)1Mmay/DboJ Camk2a-tTA	The Jackson Laboratory	JAX: 007004
Mouse: B6;129S-*Slc6a3*$^{tm4.1(tTA)Xz}$/J DAT-tTA	The Jackson Laboratory	JAX: 027178
Mouse: B6;C3-Tg(NEFH-tTA)8Vle/J NEFH-tTA	The Jackson Laboratory	JAX: 025397
Mouse: B6.Cg-Tg(Scg2-tTA)1Jt/J Scg2-tTA	The Jackson Laboratory	JAX: 008284
Mouse: B6;129S-*Rorb*$^{tm1.1(cre)Hze}$/J Rorb-tTA	The Jackson Laboratory	JAX: 023526
Mouse: B6.129P2(Cg)-*Gt(ROSA)26Sor*$^{tm1(tTA)Roos}$/J ROSA-LNL-tTA	The Jackson Laboratory	JAX: 011008
Mouse: B6.Cg-GT(ROSA)26Sor-tm9 (CAG-tdTomato)Hze/JAi9	The Jackson Laboratory	JAX: 007909
Mouse: B6;129S-Gt(ROSA)26Sortm65.1 (CAG-tdTomato)Hze/JAi65	The Jackson Laboratory	JAX: 021875
Mouse: B6.Cg-*Igs7*$^{tm62.1(tetO-tdTomato)Hze}$/J Ai62	The Jackson Laboratory	JAX: 022731

Continued

REAGENT or RESOURCE	SOURCE	IDENTIFIER
Mouse: B6.Cg-*Igs7*$^{tm90.1(tetO-COP4^*/EGFP)Hze}$/J Ai90	The Jackson Laboratory	JAX: 024100
Mouse: B6;129S6-*Igs7*$^{tm93.1(tetO-GCaMP6f)Hze}$/J Ai93	The Jackson Laboratory	JAX: 024103
Software and algorithms		
ImageJ	National Institutes of Health	https://imagej.nih.gov/ij/download.html
Fiji software	GPL v2, Fiji	http://fiji.sc/Fiji
OriginPro2021	OriginLab	https://www.originlab.com/2021

RESOURCE AVAILABILITY

Lead contact

Further information and requests for resources and reagents should be directed to and will be fulfilled by the Lead Contact, Yongling Zhu (yongling-zhu@northwestern.edu).

Materials availability

Plasmids generated in this study have been deposited to Addgene. Please see key resources table for unique identifiers.

Data and code availability

- All data reported in this paper will be shared by the lead contact upon request.
- This paper does not report original code.
- Any additional information required to reanalyze the data reported in this paper is available from the lead contact upon request

EXPERIMENTAL MODEL AND SUBJECT DETAILS

Animal care and use

Adult mice (8–12 weeks old) of either sex maintained in C57BL/6 congenic background were used for experiments. All animal procedures were performed in accordance with the Guide for the Care and Use of Laboratory Animals as adopted and promulgated by the US National Institutes of Health. All procedures for testing and handling were approved by the Institutional Animal Care and Use Committee of Northwestern University. Animals were group housed with 14-hr light /10-hr dark Light/Dark cycle. Food and water were provided *ad libitum*.

HEK 293T cells culture

HEK-293T cells were purchased from ATCC (CRL-11268). They were maintained in CO2 incubator at 37°C with 5% CO2. The cell culture media contains Dulbecco's modified Eagle's medium (DMEM) (Corning, 10-013-CM) supplied with 10% fetal bovine serum (Corning, 35-011-CV) and Penicillin-Streptomycin (Gibco 15140122, 100 units/mL of penicillin and 100 μg/mL of streptomycin). Cell passage was performed by trypsinization with 0.050% trypsin-EDTA (Gibco, 25300-054). After trypsinization, cells were seeded onto 15-cm dishes and grew in adherent condition.

METHOD DETAILS

Molecular cloning

Standard molecular cloning methods were used to construct AAV plasmids. pAAV-CBA-C$_{on}$F$_{on}$-EYFP-WPRE was constructed by subcloning BamHI/XhoI fragment from Addgene #55650 into AAV backbone containing CBA promoter (cytomegalovirus/chicken beta-actin hybrid promoter). The CBA promoter, also named CAG promoter, was initially cloned from Addgene #11160. The pAAV-EF1a-DIO-EGFP-WPRE was constructed on the backbone of pAAV-Ef1a-DIO eNpHR 3.0-EYFP (Addgene #26966). The pAAV-EF1a-fDIO-tdtomato-WPRE was made based on pAAV-Ef1a-fDIO-EYFP (Addgene #55641) by replacing EYFP with tdTomato.

Viral packaging and titering

AAVs were produced in-house using Polyethylenimine (PEI) transfection of HEK293 cells in adherent cell culture with AAV cis, AAV trans, and adenovirus helper plasmid pAdΔF6 (Gray et al., 2011). AAVs from cells pellets and media were collected 72 h post transfection and purified by iodixanol (Optiprep, Sigma; D1556) gradient ultracentrifugation as previously described (Zolotukhin et al., 1999). Viruses were concentrated and formulated in PBS. GelGreen® dye (Biotium, Fremont, CA) was used to titer AAV preparations

([Xu et al., 2020](#)). This method provides a fast (~30 min) and reliable strategy for AAV titration. Fluorescence was read with plate reader (Cytation 3).

Stereotaxic injections

Sterotaxic injection was performed on adult mice using Neurostar Robot Stereotaxic system (Tubingen, Germany). Animals remained anesthetized with isoflurane provided through nose cone during the whole surgical procedure. A micropipette connected to a Nanoject III Injector was used to inject AAV viral vectors at speed of 0.1 μL/min into the different brain regions. AAV9-C_{on}/F_{on}-EYFP (5–8 x 10^{12} gc/mL, 0.2 μL–0.3 μL/injection) or a mixture of AAV9-DIO-EGFP/AAV9-fDIO-tdTomato (1 × 10^{13} gc/mL for each, equal volume mix, 0.2 μL–0.3 μL/injection) was injected into 44 brain structures with their stereotaxic coordinates listed in [Table S6](#). For retrograde labeling from the LHb or DG, AAV2-retro-C_{on}/F_{on}-EYFP (5 × 10^{12} gc/mL, 0.1 μL/injection) or a mixture of AAV2-retro-DIO-EGFP/AAV2-retro-fDIO-tdTomato (3 × 10^{12} gc/mL for AAV2-retro-DIO-EGFP, 5 × 10^{12} gc/mL for AAV2-retro-fDIO-tdTomato, equal volume mix, 0.1 μL/injection) was injected to the LHb (*AP*:-1.6; *ML*:+/−0.3; *DV*:3.0) and DG (*AP*:-2.1; *ML*:+/−1.1; *DV*:2.2). 21–28 days after injection, animals were euthanized and the brains were fixed for immunohistochemistry and imaging analysis.

Immunohistochemistry and imaging

Mice were euthanized, and brains were fixed with 4% paraformaldehyde. After fixation, coronal brains were sectioned with a vibratome at 80-μm thick sections, and washed with a modified phosphate buffer (PB) containing 0.5% Triton X-100 and 0.1% NaN3, pH 7.4, and then blocked for 1 day in modified PB containing 5% donkey serum. Brain slices were then incubated with primary antibody overnight at 4$°$C. After wash, brain slices were incubated with donkey secondary antibody for another night at 4$°$C. The primary antibodies used were as follows: goat anti-GFP (1:500, Abcam ab5450), rabbit anti-RFP (1:500, Rockland 600-401-379), mouse anti-Pvalb (1:250, Swant 235), rat anti-SST (1:10, Millipore MAB354), rabbit anti-VIP (1:1000, ImmunoStar, 20,077). Secondary antibodies were conjugated to Alexa Fluor 488 or Cy3 (Jackson ImmunoResearch). All secondary antibodies were used at a dilution of 1:200.

Brains sections were mounted on glass slides (25 × 50 mm) with fluoroshield mounting medium with DAPI (EMS 17989). Epifluorescence images of brain sections were captured with KEYENCE BZ-X710 microscope (KEYENCE CORPORATION, Itasca, IL) with 4x or 10x objectives. A Zeiss LSM-510 Meta confocal microscope (25x objective) were used when higher magnification is required for cell morphology analysis.

In situ Hybridization/RNAscope

In situ hybridization was performed using the RNAScope. Multiplex Fluorescent Reagent kit v2 (Advanced Cell Diagnostics). Briefly, brains from adult mice (3 months old) were fixed in 4% PFA for 1 day, embedded in paraffin and then sectioned at 5 μm thickness onto glass slides. Brain sections were then deparaffinized in xylene, rehydrated in ethanol, and processed for RNA *in situ* hybridization following manufacturer's recommendations. The following probes were used in this study. 1) ACD Cat# 319171-C2 Mm-Slc17a6-C2 - Mus musculus solute carrier family 17, member 6, VGLUT2. 2) ACD Cat# 319191 Mm-Slc32a1- Mus musculus solute carrier family 32, member 1, VGAT.

QUANTIFICATION AND STATISTICAL ANALYSIS

At least 3 brains were examined for each combinational mouse line. Epifluorescence images of brain series acquired by KEYENCE system were individually registered to their closest corresponding Allen Mouse Brain Reference Atlas (https://mouse.brain-map.org/static/atlas) level. Afterwards, each brain image was matched to Allen brain diagram of corresponding levels, with anatomical landmarks and DAPI stain as guides to determine the identity of nucleus of interest. Brain regions were defined with reference to the Allen Mouse Brain Reference Atlas, with the Paxinos and Franklin atlas ([Paxinos and Franklin, 2004](#)) as a secondary resource. Cell counting was performed manually using Adobe Photoshop or Image J.

All data are expressed as the mean ± SEM. Data collection and analysis were not performed blind to the conditions of the experiments. No statistical analysis was performed in this study. No data points were excluded. No statistical methods were used to predetermine sample sizes, but our sample sizes are similar to those reported in previous publication.
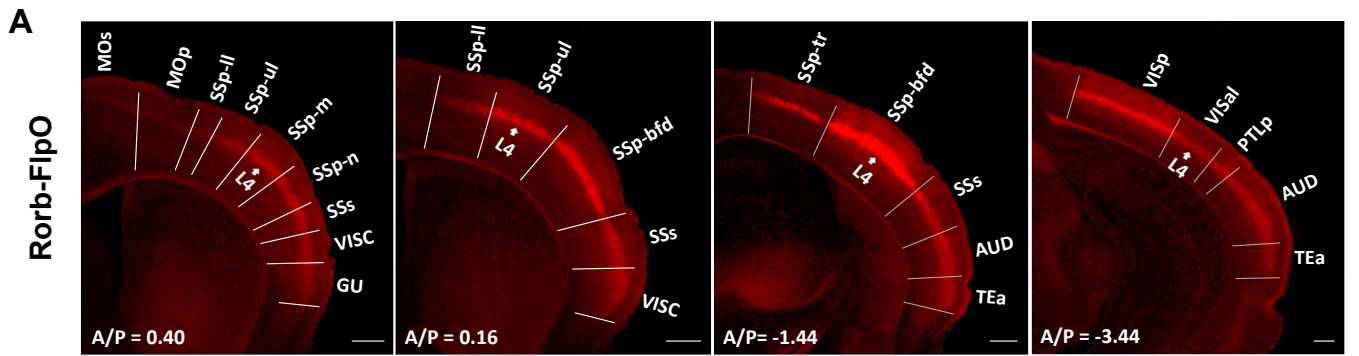
Supplemental information

Intersectional mapping of multi-transmitter

neurons and other cell types in the brain

Jian Xu, Andrew Jo, Raina P. DeVries, Sercan Deniz, Suraj Cherian, Idris Sunmola, Xingqi Song, John J. Marshall, Katherine A. Gruner, Tanya L. Daigle, Anis Contractor, Talia N. Lerner, Hongkui Zeng, and Yongling Zhu

A

	Isocortex	Striatum & Pallidum	Amygdala	Claustrum, Endopiriform nucleus	Hippocampal formation	Olfactory areas	Thalamus	Hypothalamus	Midbrain
Rorb-FlpO	SSp(L4), SSs(L4), VIS(L4), AUD(L4), VISC(L4), GU(L4)								
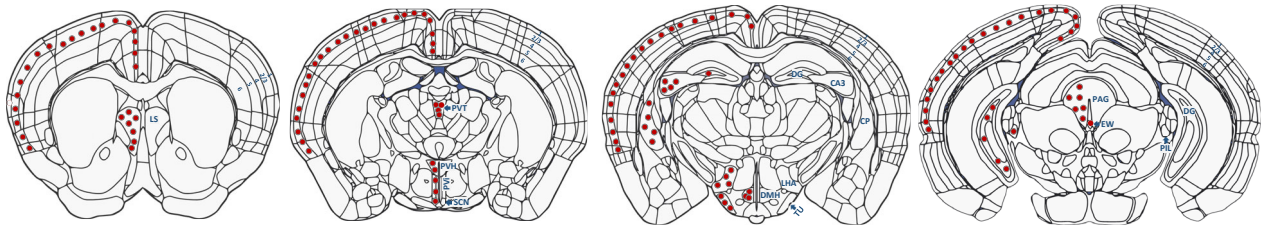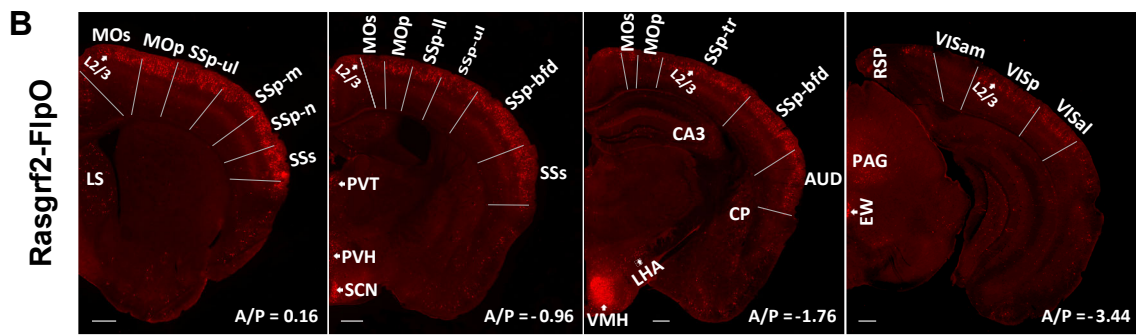
B

	Isocortex	Striatum & Pallidum	Amygdala	Claustrum, Endopiriform nucleus	Hippocampal formation	Olfactory areas	Thalamus	Hypothalamus	Midbrain
Rasgrf2-FlpO	MO(L2/3), SSp (L2/3), SSs(L2/3), VIS(L2/3), AUD(L2/3), ACA (L2/3), RSP(L2/3)	CP, LS			CA3, DG	MOB, AOB	PVT	PVH, PVi, DMH, LHA, SCN, TU	PAG, EW, PIL

Figure S1. Flp expression patterns in Rorb-FlpO and Rasgrf2-FlpO drivers. Related to Figure 1.

(A) Distributions of Flp-expressing cells in Rorb-FlpO driver.

(B) Distributions of Flp-expressing cells in Rasgrf2-Flp driver.

Each Flp driver was crossed with CMV-Cre and Ai65 mice.

Scale bars: 500μm.

A Dlx5/6-FlpO

B Nkx2-FlpO

C

	Isocortex	Striatum & Pallidum	Amygdala	Claustrum, Endopiriform nucleus	Hippocampal formation	Olfactory areas	Thalamus	Hypothalamus	Midbrain
Dlx5/6-FlpO	pan	pan	pan		pan	MOB, AON, TR	RT	ZI, DMH, LHA, ARH	
Nkx2-FlpO	pan	pan	pan		pan	pan		astrocytes	

D DAT-tTA

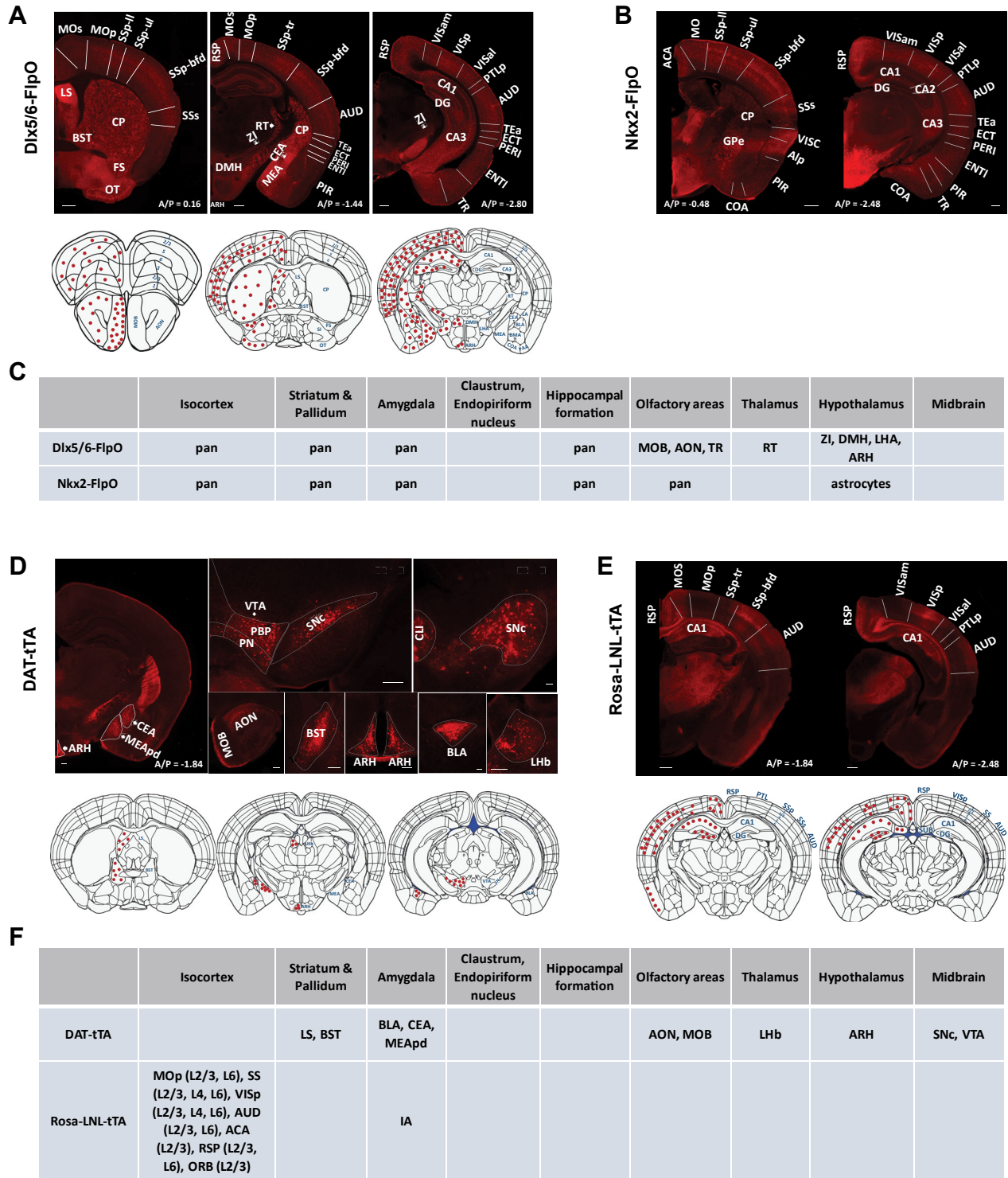**E** Rosa-LNL-tTA

F

	Isocortex	Striatum & Pallidum	Amygdala	Claustrum, Endopiriform nucleus	Hippocampal formation	Olfactory areas	Thalamus	Hypothalamus	Midbrain
DAT-tTA		LS, BST	BLA, CEA, MEApd			AON, MOB	LHb	ARH	SNc, VTA
Rosa-LNL-tTA	MOp (L2/3, L6), SS (L2/3, L4, L6), VISp (L2/3, L4, L6), AUD (L2/3, L6), ACA (L2/3), RSP (L2/3, L6), ORB (L2/3)		IA						

Figure S2. Flp expression patterns in Dlx5/6-FlpO and Nkx2-FlpO drivers, and tTA expression patterns in DAT-tTA and Rosa-LNL-tTA drivers. Related to Figures 1, 2.
(A, B) Distributions of Flp-expressing cells in Dlx5/6-FlpO (A) and Nkx2-FlpO (B) drivers.
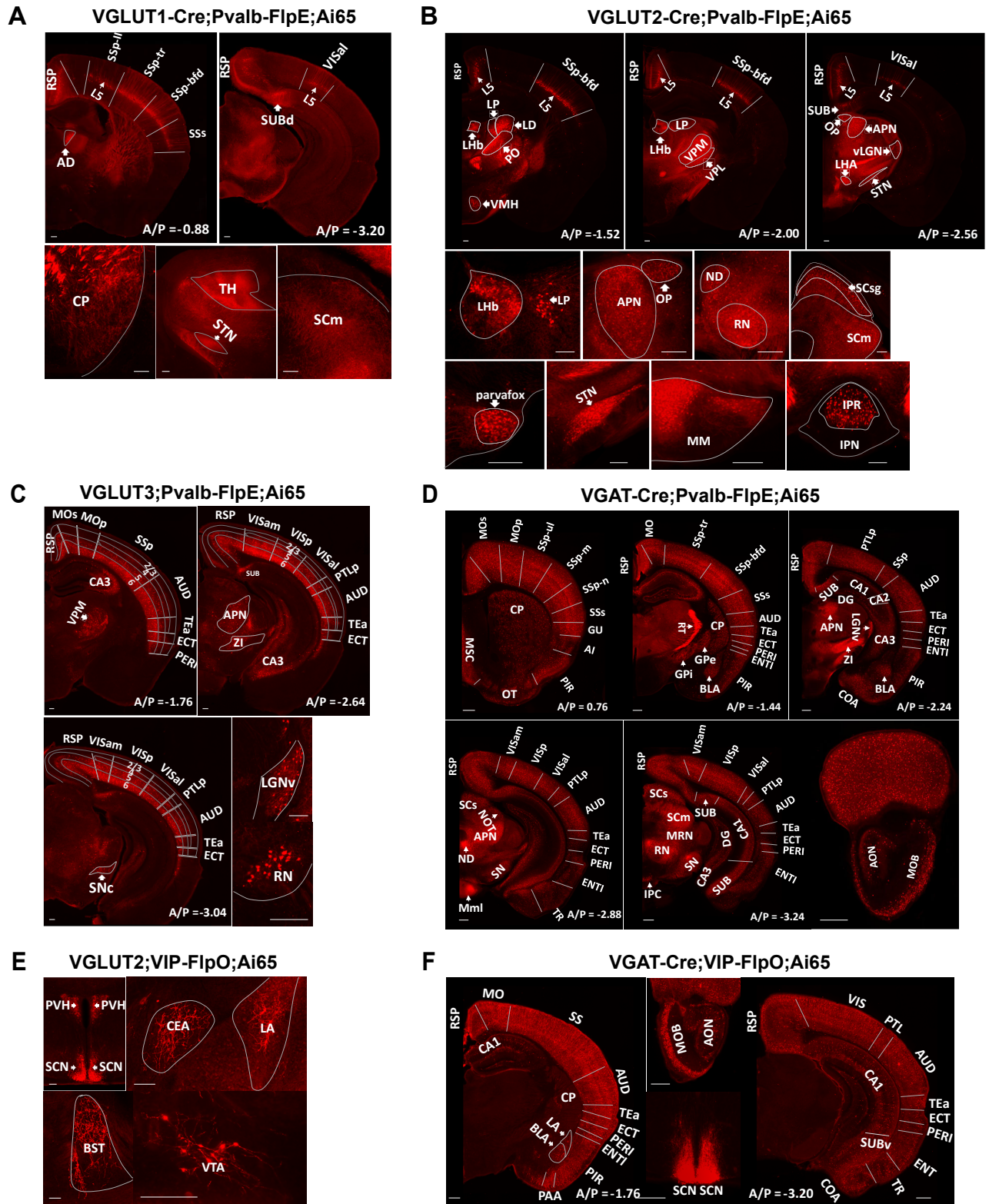(C) Summary of Flp expression patterns.
(D, E) Distributions of tTA-expressing cells in DAT-tTA (D) and Rosa-LNL-tTA (E) drivers.
(F) Summary of tTA expression patterns.
Each Flp driver was crossed with CMV-Cre and Ai65 mice. Each tTA driver was crossed with CMV-Cre and Ai62 mice.
Scale bars: 500µm (A, B, and E), 200µm (D).

Figure S3. Distributions of Pvalb and VIP neurons probed with intersectional strategies. Related to Figure 1.
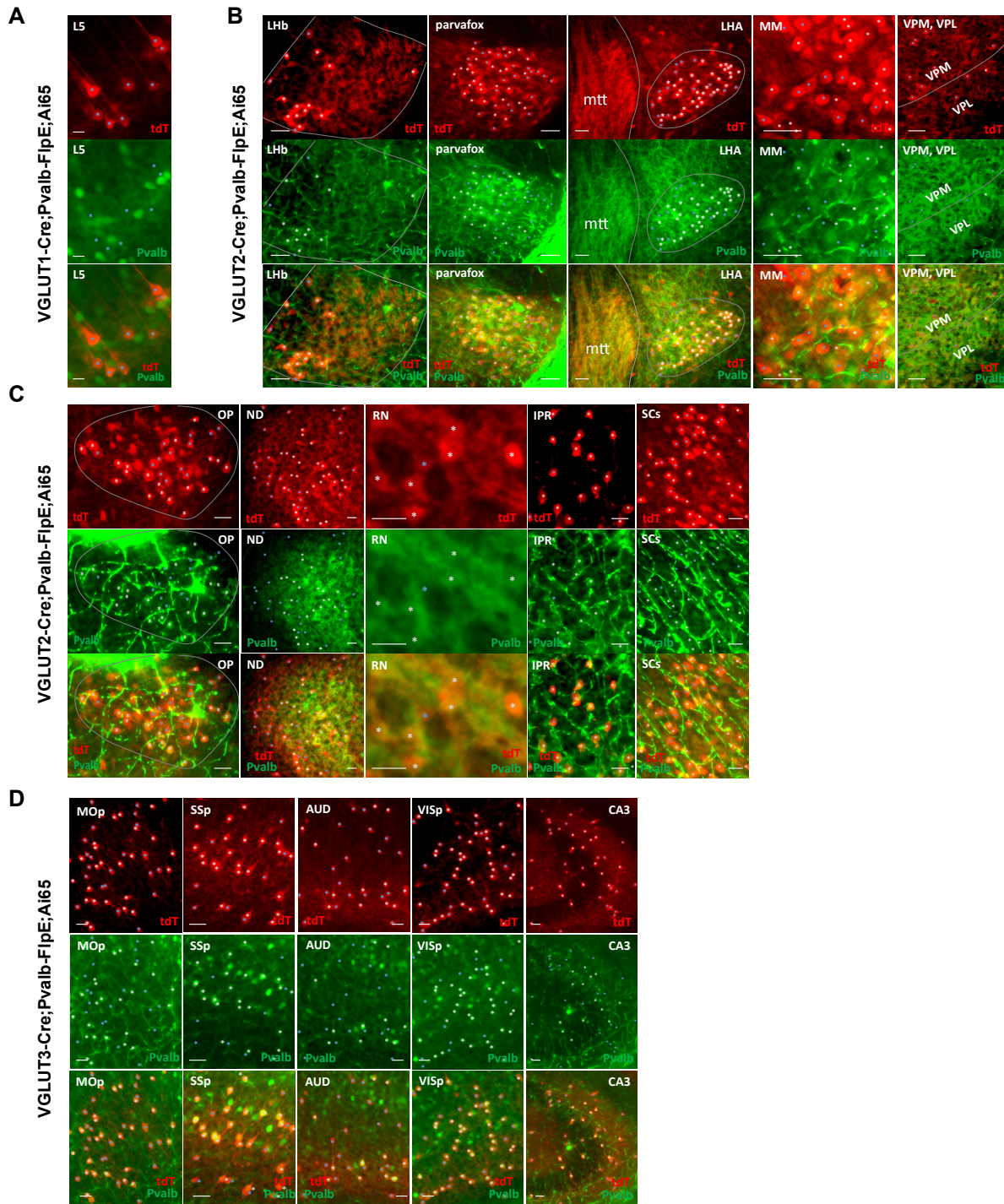
(A-D) Representative images of labeled neurons in VGLUT1-Cre;Pvalb-FlpE;Ai65 (A), VGLUT2-Cre; Pvalb-FlpE;Ai65 (B), VGLUT3-Cre;Pvalb-FlpE;Ai65 (C), and VGAT-Cre;Pvalb-FlpE;Ai65 (C) mice.

(E, F) Representative images of labeled neurons in VGLUT2-Cre;VIP-FlpO;Ai65 (E) and VGAT-Cre; VIP-FlpO;Ai65 (F) mice.

Scale bars: 200μm (A, B, C, and E), 500μm (D and F).

Figure S4. Glutamatergic Pvalb neurons probed with intersectional strategies. Related to Figure 1.
(A) The L5 cortical neurons labeled in VGLUT1-Cre;Pvalb-FlpE;Ai65 intersection showed no or low Pvalb expression.
(B) Pvalb-expressing glutamatergic neurons in the thalamus and hypothalamus probed with VGLUT2-Cre; Pvalb-FlpE;Ai65.
(C) Pvalb-expressing glutamatergic neurons in the midbrain probed with VGLUT2-Cre;Pvalb-FlpE;Ai65.
(D) VGLUT3-Cre;Pvalb-FlpE;Ai65 labeled Pvalb-expressing neurons in L5, L6 of the isocortex, and in the hippocampal CA3.
White stars: cells co-labeled with tdTomato (Ai65) and antibody against Pvalb. Blue star: cells labeled with tdTomato (Ai65), but not with Pvalb antibody.
Scale bars: 20µm (A), 50µm (B, C, and D).
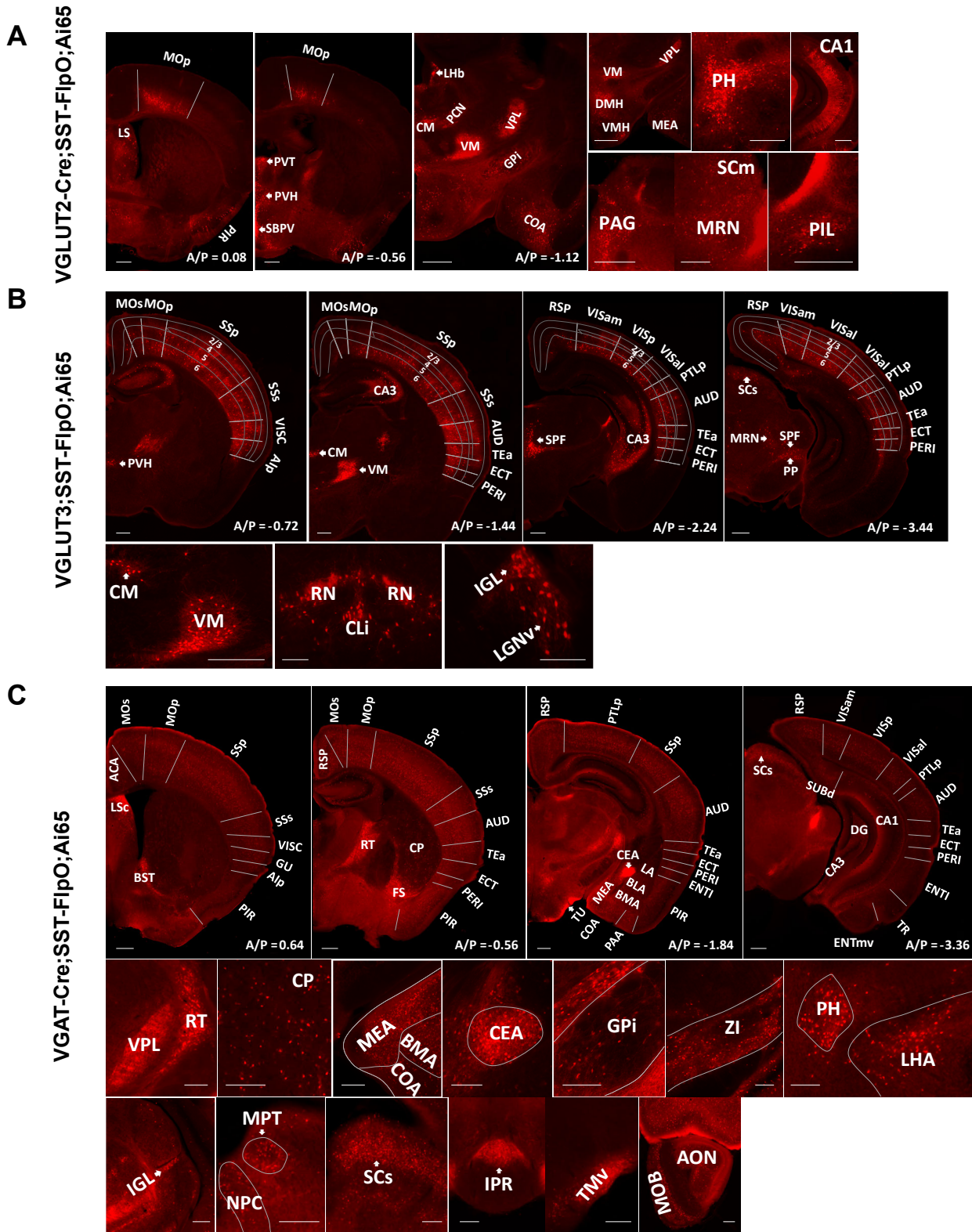
Figure S5. Distributions of SST neurons probed with intersectional strategies. Related to Figure 1.

Representative images of labeled neurons in VGLUT2-Cre;SST-FlpO;Ai65 (A), VGLUT3-Cre; SST-FlpO;Ai65 (B) and VGAT-Cre;SST-FlpO;Ai65 (C) mice.

Scale bars: 500μm (A, B, and C top), 250μm (C middle and bottom).
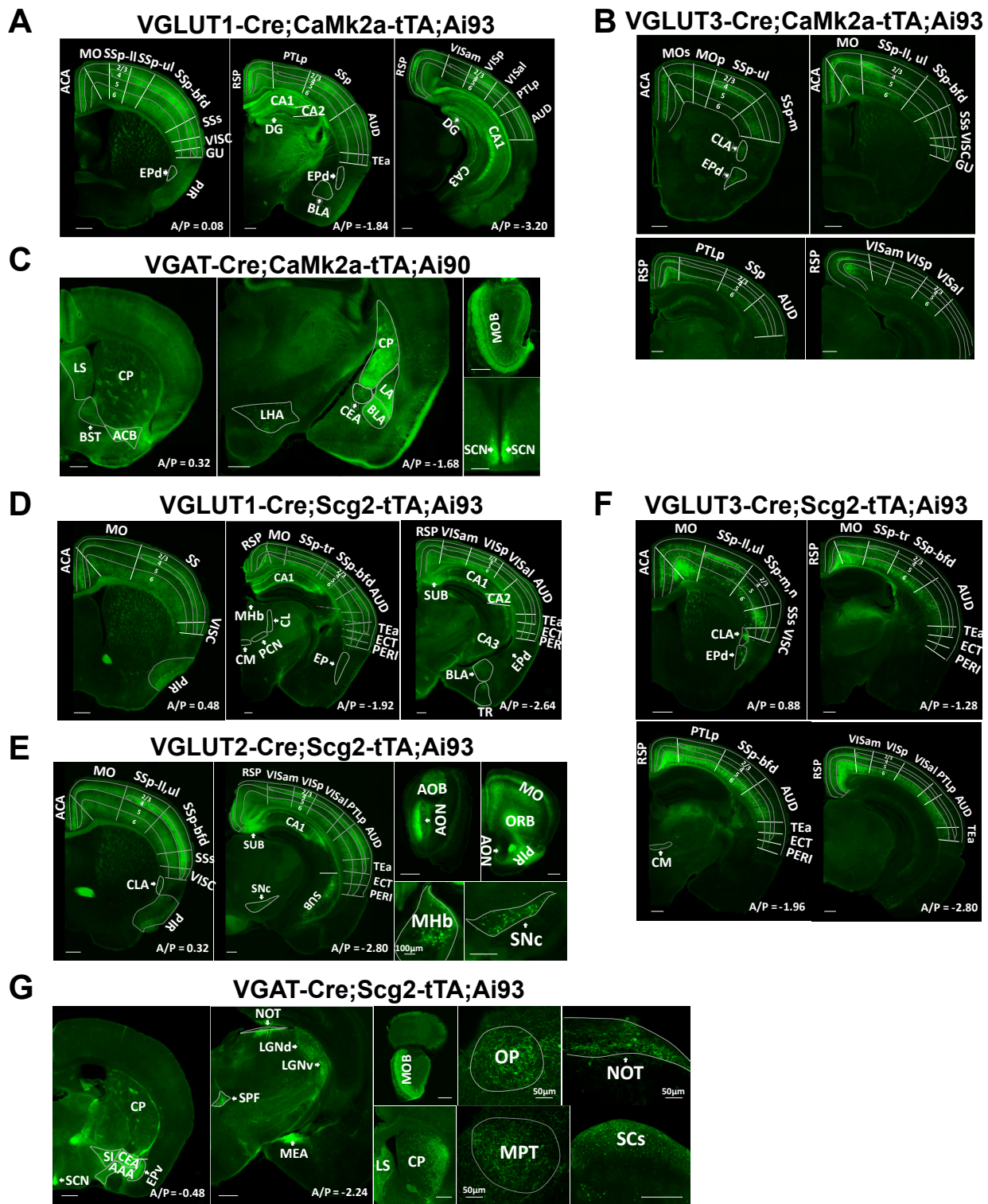
Figure S6. Distributions of labeled neurons in CaMk2a-tTA and Scg2-tTA. Related to Figure 2.

(A-C) Representative images of labeled neurons in VGLUT1-Cre;CaMk2a-tTA (A), VGLUT3-Cre;CaMk2a-tTA (B), and VGAT-Cre;CaMk2a-tTA (C) intersections.

(D-G) Representative images of labeled neurons in VGLUT1-Cre;Scg2-tTA (D), VGLUT2-Cre;Scg2-tTA (E), VGLUT3-Cre;Scg2-tTA (F), and VGAT-Cre;Scg2-tTA (G) intersections.

Scale bars: 500µm (A, B, C, D, E, F, and G).
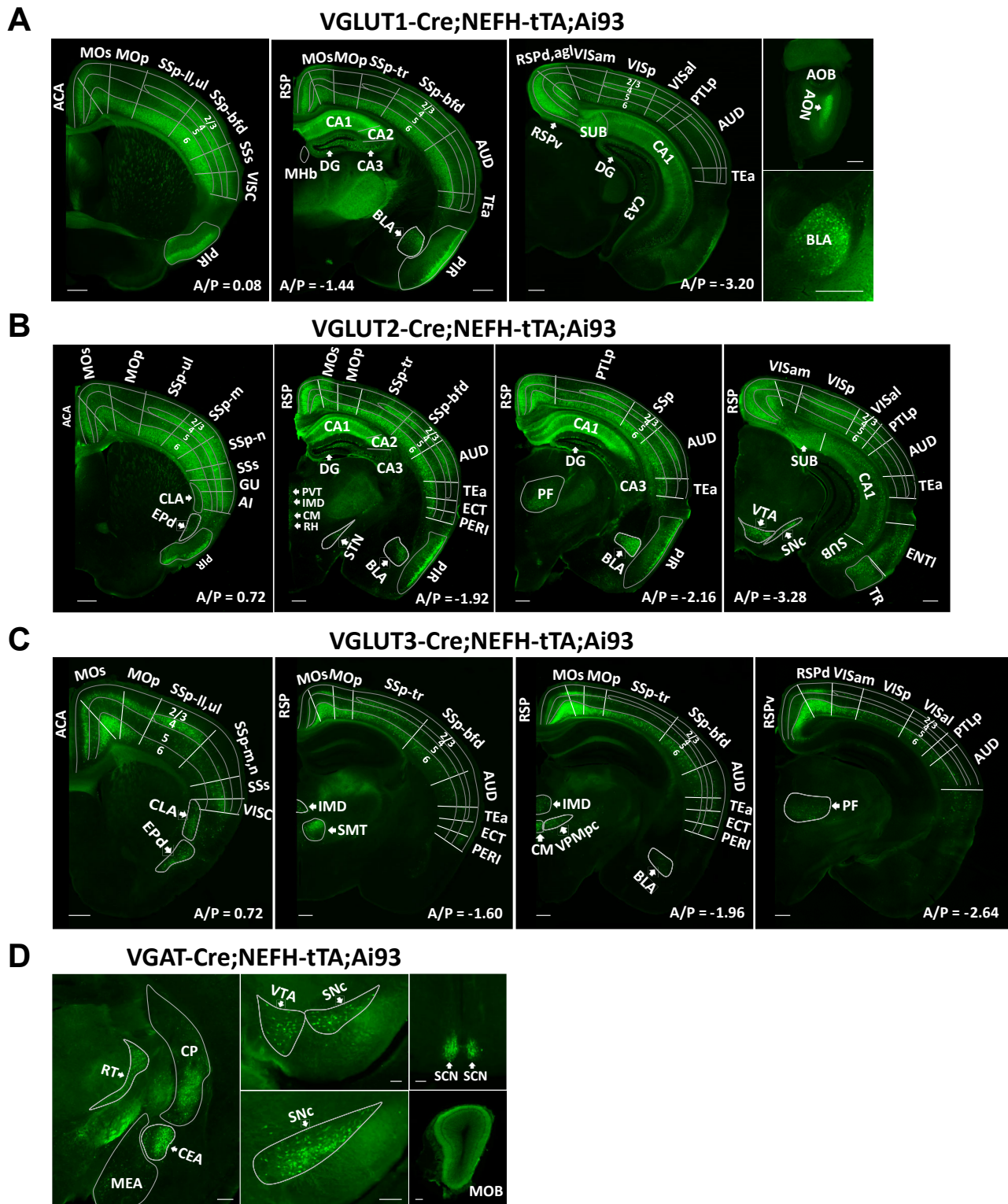
Figure S7. Distributions of labeled neurons in NEFH-tTA. Related to Figure 2.
Representative images of labeled neurons in VGLUT1-Cre;NEFH-tTA (A), VGLUT2-Cre; NEFH-tTA (B), VGLUT3-Cre;NEFH-tTA (C), and VGAT-Cre;NEFH-tTA (D) intersections. Scale bars: 500μm (A, B, and C), 250μm (D).
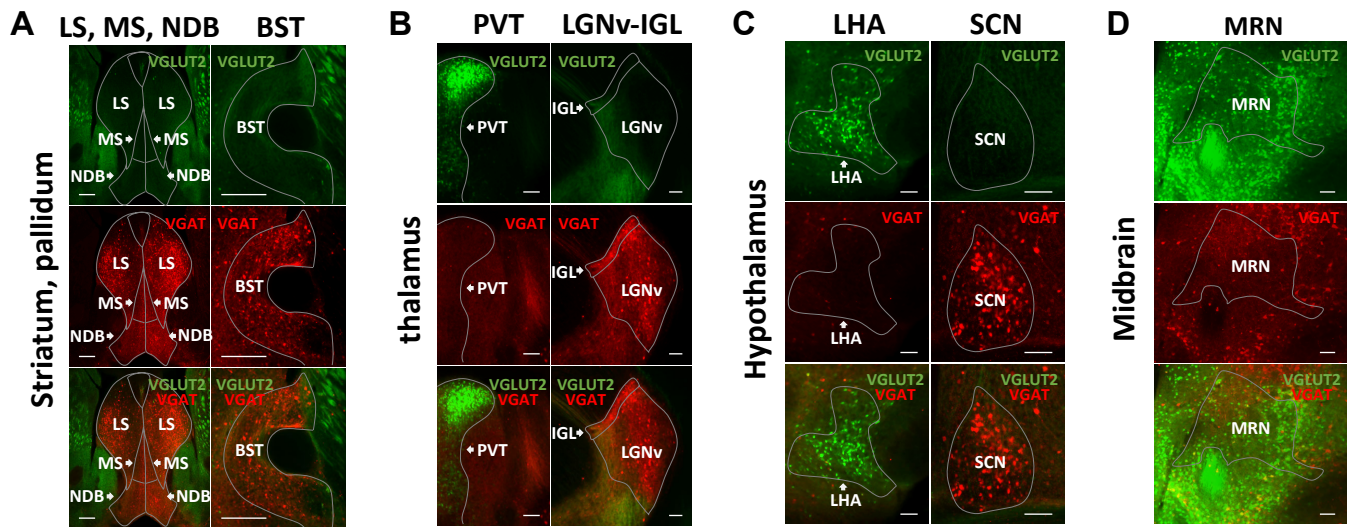
Figure S8. LHb-projecting regions provided glutamatergic innervations alone, GABAergic innervations alone or mixed innervations originated from sole glutamatergic and sole GABAergic neurons. Related to Figure 6.

Retrograde labeling of LHb-projecting neurons was performed by injecting AAV2-retro-DIO-EGFP /AAV2-retro-fDIO-tdT mix into the LHb of VGLUT2-Cre;VGAT-FlpO mice. Representative images of labeled structures that have been reported by previous studies.

Scale bars: 500μm (A), 100μm (B, C, and D).

Table S2. GABAergic and glutamatergic neurons in Pvalb-FlpE, SST-FlpO, VIP-FlpO drivers. Related to Figure 1B-D.

	Cerebral cortex	Striatum & Pallidum	Amygdala	Claustrum, Endopiriform nucleus	Hippocampal formation	Olfactory areas	Thalamus	Hypothalamus	midbrain
VGLUT1-Cre/Pvalb-FlpE	SSp (L5), VISal (L5), RSP (L2/3, L5)				SUB	AON	AD, LD		
VGLUT2-Cre/Pvalb-FlpE	SSp (L5), VISal (L5), RSP (L5)	SF, SI, MS, GPi			SUB	AON	AD, AV, LD, LP, PO, CL, PCN, LGNv, LHb*, VPM, VPL	MPO, LPO, VMH, STN, MM*, parvafox nucleus*, LHA*	APN, PPT, OP*, IPR*, SCs-sg*, SCs-op*, SCm, ND*, RN*, MRN
VGLUT3-Cre/Pvalb-FlpE	L5, L6 of all regions*				CA3*, SUB		LGNv	SNc, ZI	APN, RN, III
VGAT-Cre/Pvalb-FlpE	Pan*	CP*, FS*, GPe*, GPi*, MS*, NDB*, OT*, SI*	LA*, BLA*, BMA*, COA*	EPd*, EPv*	CA1*, CA2*, CA3*, DG*, SUB*	MOB*, AON*, PIR*, TR*	RT*, AD*, LD*, AV*, LGNv*	ADP*, MPO*, MA*, STN*, ZI*	APN*, SNr*, ND*, SCs*, SCm*, MRN*, IPC*, RN*
VGLUT1-Cre/SST-FlpO	MOp (L6)		BLA, PAA, COA		CA1-sp (ventral), CA3-sp (dorsal)	MOB, AON			
VGLUT2-Cre/SST-FlpO	MOp (L6)	LSc, LSr, GPi*	MEA, COA, PAA		CA1-sp (ventral), CA3-sp (dorsal)	AON	PVT, RE, CM, PCN, LHb*, VPL, VM, SPF, PIL, PP	MPO, PVH, PVa, SBPV, RCH, DMH, VMH, TU, PH, TMv	PRC, MRN, SCm, VTA*
VGLUT3-Cre/SST-FlpO	L5, L6 of all regions				CA3-so*		CM, VM, SPA, SPF, LGNv, IGL, PIL, PP	PVH	MRN, PN, SCs
VGAT-Cre/SST-FlpO	Pan*	CP*, FS*, SI*, OT*, LSc*, LSr*, LSv*, BST*, GPi*	CEA*, LA*, BLA*, BMA*, MEA*, COA*, PAA*, PA*	EPv*, EPd*	CA1-so*, CA2-so*, CA3-so*, DG-po*, SUB*	MOB*, AON*, TR*, PIR*	RT*, SPF*, LGNv*, IGL*	ZI*, LHA*, PVp*, TMv*, ARH*, TU*	IPR*, MPT*, NPC*, SCs*, SCm*, VTA*
VGLUT2-Cre/VIP-FlpO		BST	CEA, LA					PVpo, PVH, SCN	VTA
VGAT-Cre/VIP-FlpO	MO (L2/3)*; SS*, VIS*, AUD (L2/3, L4)*; ACA*, RSP (L2/3)*	CP*, BST*	CEA*, LA*, BLA*, COA*, PAA*, PA*		CA1*, DG*, SUB*	MOB*, AON*		SCN*	

*Regions containing labeled neurons expressing Pvalb, SST, or VIP, determined with immunochemistry.

Table S3. GABAergic and glutamatergic neurons in CaMk2a-tTA, Scg2-tTA, NEFH-tTA drivers. Related to Figure 2B-D.

	Cerebral cortex	Striatum & Pallidum	Amygdala	Claustrum, Endopiriform nucleus	Hippocampal formation	Olfactory areas	Thalamus	Hypothalamus	midbrain
VGLUT1-Cre/CaMk2a-tTA	MO(L2/3, L6), SS, AUD(L2/3, L4, L6), VIS(L4, L6), ACA, RSP(L2/3, L6)		BLA, COA	EP	pan	AON, PIR			
VGLUT2-Cre/CaMk2a-tTA	MO(L2/3, L6), SS, AUD(L2/3, L4, L6), VIS(L4, L6), ACA, RSP(L2/3, L6)		BLA, COA	EP	pan	AON, PIR			
VGLUT3-Cre/CaMk2a-tTA	MO(L2/3, L6), SS(L4, L5, L6), VIS, AUD(L6), ORB(L2/3, L5), ACA, RSP(L2/3, L6)			CLA, EP	ENTl	TR			
VGAT-Cre/CaMk2a-tTA		CP, ACB, LS, SI, OT, BST, FS	CEA, LA, BLA			MOB, AOB		SCN, LHA	
VGLUT1-Cre/Scg2-tTA	MO(L2/3, L5, L6), SS(L2/3, L4, L5, L6), VIS,AUD(L4, L6), ORB(L2/3, L5), ACA(L2/3, L5, L6), RSP(L2/3, L6)		BLA	EP	CA1, CA3, DG, SUB, POST, PRE, PAR, ENTl	AON, PIR, TR	MHb, CM, PCN, CL		
VGLUT2-Cre/Scg2-tTA	MO(L2/3, L5, L6), SS(L2/3, L4, L5, L6), VIS, AUD(L4, L6), ORB(L2/3, L5), ACA(L2/3, L5, L6), RSP(L2/3, L6)			CLA	CA1, SUB, POST, PRE, PAR. ENTl	AON, AOB, PIR	MHb		SNc
VGLUT3-Cre/Scg2-tTA	MO(L2/3, L6), SS(L4, L5, L6), VIS, AUD(L6), ORB(L2/3, L5), ACA, RSP(L2/3, L6)			CLA, EP			CM		
VGAT-Cre/Scg2-tTA		CP, LS, SI, FS, OT, BST	CEA, MEA, AAA	EP		MOB	LGNd, LGNv,	SCN	OP, MPT, NOT, SCs, SPF, SNc
VGLUT1-Cre/NEFH-tTA	MOs(L2/3, L6), MOp (L6), SS, VIS, AUD (L4, L6), ORB(L5), ACA, RSP (L2/3, L6)		BLA	EP	pan	AOB, AON, PIR, TR	MHb		
VGLUT2-Cre/NEFH-tTA	MO(L2/3, L6), SS, VIS, AUD (L4, L6), ORB(L5), ACA, RSP (L2/3, L6)		BLA	EP	pan	AON, PIR, TR	PVT, IMD, CM, RE,PF	STN	VTA, SNc
VGLUT3-Cre/NEFH-tTA	MO (L2/3, L6), SS(L4, L5, L6), VIS, AUD (L6), ORB(L2/3, L5), ACA(L2/3, L6), RSP(L6)			CLA, EP			IMD, CM, SMT, VPMpc,PF		
VGAT-Cre/NEFH-tTA		CP, ACB, GPe, LS, MS, NDB, BST, FS	CEA, MEA			MOB	RT	SCN	VTA, SNc

Table S4. Neurons labeled in Cre/tTA lines. Related to Figure 2F-I.

	Cerebral cortex	Striatum & Pallidum	Amygdala	Claustrum, Endopiriform nucleus	Hippocampal formation	Olfactory areas	Thalamus	Hypothalamus	midbrain
CCK-Cre/CaMk2a-tTA	MO(L2/3, L6), SS, VIS(L4, L6), AUD(L6), ACA, RSP(L2/3, L6)	CP	LA, BLA, COA	EP	CA1-sp, CA3-sp, DG-sg	PIR, TR			
CCK-Cre/Scg2-tTA	MO(L6), SS, VIS(L4, L6), AUD(L6), RSP(L2/3)				CA1-sp, CA3-sp, DG-sg, DG-po	PIR			
SST-Cre/CaMk2a-tTA	MOp(L6)	CP, LSc, BST, FS, OT	LA, CEA, MEA, COA		CA3-sp, CA1-sp (ventral), SUB, ENTl	PIR, TR			
SST-Cre/Scg2-tTA	MOp(L6)	CP, LSc, BST, FS	MEA		SUBv-sp, ENTl	AON, PIR			SCs
Tac1-Cre/Scg2-tTA	MO(L4, L6), SSp(L4. L6), RSP(L2/3)	CP	CEA		SUBv-sp, POST, PRE		MHb		SCs
Scnn1a-Cre/CaMk2a-tTA	SS, VIS, AUD(L4), RSP(L2/3)								
Scnn1a-Cre/Scg2-tTA	SSp (L4, L5), SSs, AUD, VISp(L4), ACA (L2/3), RSP (L2/3, L6)	BST	MEA, BMA, COA, PA		CA1-sp, SUB-sp, POST(L2), PRE(L2), PAR(L2), ENTl		RE		
Penk-Cre/CaMk2a-tTA	RSP (L2/3, L5)	CP, BST	BLA, CEA, MEA		CA1-sp, SUB	MOB			
Penk-Cre/Scg2-tTA	MO(L2/3, L6), SS, AUD, VIS, ACA, RSP(L2/3, L6)				CA1-sp	PIR			
L7-Cre/CaMk2a-tTA	MO(L2/3), SSp(L2/3, L4/L5 border), AUD, VIS(L2/3, L4), ACA (L2/3), RSP(L2/3, L5, L6)				CA1-sp, DG-sg, SUB, ENTl				

Table S5. Fractions of LHb-projecting neurons expressing VGLUT2 only, VGAT only, or VGLUT2 and VGAT. Related to Figure 5D.

	VGLUT2 only	VGAT only	VGLUT2 and VGAT
GPi	5% ± 1%	1% ± 0%	94% ± 6%
IF	14% ± 2%	0 ± 0%	86% ± 9%
PN	29% ± 3%	28% ± 2%	43% ± 3%
PBP	50% ± 4%	18% ± 2%	32% ± 3%
RLi	53% ± 6%	4% ± 1%	43% ± 5%
CLi	32% ± 3%	1% ± 0%	67% ± 7%
SCs	70% ± 8%	7% ± 1%	23% ± 2%
MPT	77% ± 8%	0 ± 0%	23% ± 2%
MEApd-a	40% ± 5%	23% ± 3%	37% ± 4%
LPO	41% ± 4%	27% ± 3%	32% ± 3%
SI	15% ± 1%* 20% ± 3%**	73% ± 8%* 32% ± 3%**	12% ± 2%* 48% ± 5%**
MA	32 ± 4%	45 ± 5%	23 ± 3%
EW	38% ± 5%	24% ± 3%	38 ± 4%

N= 5 brains. Shown are means ± SEM.

*A/P = 0.13mm,

** A/P = -0.77 mm

Table S6. Brain structures and their stereotaxic coordinates for AAV9-C$_{on}$/F$_{on}$-EYFP injection and AAV9-DIO-EGFP/AAV9-fDIO-tdTomato injection. Related to: STAR METHODS/Method details/Stereotaxic Injections

ACA	*AP*:-0.5; *ML*:+/-0.3; *DV*:1.4	MPO	*AP*:0; *ML*:+/-0.7; *DV*:5.0
AHN	*AP*:-0.7; *ML*:+/-0.5; *DV*:5.1	MPT	*AP*:-2.7; *ML*:+/-0.4; *DV*:2.1
AUD	*AP*:-2.7; *ML*:+/-4.0; *DV*:2.4	MRN	*AP*:-3.1; *ML*:+/-0.6; *DV*:3.1
BST	*AP*:0.10; *ML*:+/-0.9; *DV*:4.1	PAA	*AP*:-1.3; *ML*:+/-3.1; *DV*:5.7
CA1	*AP*:-2.2; *ML*:+/-1.0; *DV*:1.5 *AP*:-2.6; *ML*:+/-2.7; *DV*:2.0	PALv	*AP*:0.10; *ML*:+/-1.5; *DV*:5.5
CA3	*AP*:-2.3; *ML*:+/-2.5; *DV*:2.4 *AP*:-2.5; *ML*:+/-3.0; *DV*:2.7	PIR	*AP*:1.8; *ML*:+/-2.2; *DV*:4.5
CLi	*AP*:-3.7; *ML*:+/-0; *DV*:3.7	PMv	*AP*:-2.2; *ML*:+/-0.5; *DV*:5.3
COA	*AP*:-1.3; *ML*:+/-2.5; *DV*:5.7	PP	*AP*:-3.1; *ML*:+/-2.3; *DV*:3.8
DG	*AP*:-1.8; *ML*:+/-0.8; *DV*:2.2 *AP*:-2.7; *ML*:+/-1.6; *DV*:2.0	PPT	*AP*:-2.9; *ML*:+/-0.7; *DV*:2.0
DMH	*AP*:-1.7; *ML*:+/-0.4; *DV*:5.0	PVH	*AP*:-0.7; *ML*:+/-0; *DV*:4.8
DR	*AP*:-4.0; *ML*:+/-0; *DV*:3.6	RN	*AP*:-3.1; *ML*:+/-0.8; *DV*:3.7
ENTl	*AP*:-3.1; *ML*:+/-4.0; *DV*:4.6	RSP	*AP*:-3.1; *ML*:+/-0.4; *DV*:1.1
EPd	*AP*:-0.5; *ML*:+/-3.4; *DV*:4.4	SBPV	*AP*:-0.7; *ML*:+/-0; *DV*:5.1
EW	*AP*:-3.7; *ML*:+/-0; *DV*:3.0	SCm	*AP*:-3.6; *ML*:+/-1.0; *DV*:2.2
GPi	*AP*:-1.4; *ML*:+/-1.8; *DV*:4.3	SCs	*AP*:-3.6; *ML*:+/-0.5; *DV*:1.3
IGL	*AP*:-2.3; *ML*:+/-2.2; *DV*:3.0	SNc	*AP*:-3.1; *ML*:+/-1.3; *DV*:4.3
IPN	*AP*:-3.5; *ML*:+/-0; *DV*:4.7	SPFp	*AP*:-3.1; *ML*:+/-1.8; *DV*:3.6
LHA	*AP*:-2.2; *ML*:+/-0.9; *DV*:4.9	SSp	*AP*:-0.5; *ML*:+/-3.0; *DV*:2.0
LPO	*AP*:0.3; *ML*:+/-0.8; *DV*:5.2	SUM	*AP*:-2.6; *ML*:+/-0; *DV*:5.0
MEAav	*AP*:-1.3; *ML*:+/-1.8; *DV*:5.5	VISp	*AP*:-3.0; *ML*:+/-2.4; *DV*:1.0
MEApd	*AP*:-2.0; *ML*:+/-2.0; *DV*:4.9	LGNv	*AP*:-2.3; *ML*:+/-2.5; *DV*:3.3
MO	*AP*:-0.5; *ML*:+/-0.8; *DV*:1.1	VTA	*AP*:-3.1; *ML*:+/-0.4; *DV*:4.3